scientific reports

Check for updates

OPEN

# A nano phototheranostic approach of toluidine blue conjugated gold silver core shells mediated photodynamic therapy to treat diabetic foot ulcer

Farheen Akhtar[1], Asad U. Khan[1]✉, Bushra Qazi[1], Senthilguru Kulanthaivel[2], Prashant Mishra[2], Kafil Akhtar[3] & Asif Ali[4]

**Diabetic foot infection caused by multidrug-resistant bacteria, is becoming serious problem. Moreover, polymicrobial biofilms contribute significantly to the persistent infections. In the present study, we investigated the effectiveness of novel toluidine blue conjugated chitosan coated gold–silver core–shell nanoparticles (TBO–chit–Au–AgNPs) mediated photodynamic therapy and demonstrate their use as a nontoxic antibacterial therapy to combat diabetic foot ulcer (DFU) caused by multi-drug resistant strains both in monomicrobial and polymicrobial state of infection. In vitro efficacy of TBO–chit–Au–AgNPs mediated photodynamic therapy (PDT) against polymicrobial biofilms was determined using standard plate count method and compared with that of monomicrobial biofilms of each species. Different anti-biofilm assays and microscopic studies were performed to check the efficacy of TBO–chit–Au–AgNPs mediated PDT, displayed significant decrease in the formation of biofilm. Finally, its therapeutic potential was validated in vivo type-2DFU. Cytokines level was found reduced, using nano-phototheranostic approach, indicating infection control. Expression profile of growth factors confirmed both the pathogenesis and healing of DFU. Hence, we conclude that TBO–chit–Au–AgNPs mediated PDT is a promising anti-bacterial therapeutic approach which leads to a synergistic healing of DFU caused by MDR bacterial strains.**

Type 2 diabetes mellitus (DM) has become an utmost health concern which comprised of 90–95% diabetes among worldwide population[1]. Nevertheless, immunocompromised patients identified with diabetes mellitus are more prone to be suffered from non-healing wounds[2]. It has also been reported that up to one-third of people with diabetes may develop foot ulcer during their lifetime and over 50% of these ulcers become infected. This challenge is further aggravated by the emergence of multidrug-resistance (MDR) strains induced diabetic foot infections (DFIs) which leads to increasing morbidity and mortality, and risk of lower extremity amputation (LEA) which causes low quality of life[3–6]. Furthermore, biofilm-forming MDR strains are far more impervious to antimicrobials than organisms in suspension[7–9]. It has been stated earlier that biofilms intricate up to 65% of infections, leading to severe illness with a prolonged stay in hospital settings which may increase cost of treatment as well as mortality rate[10].

The most commonly found microorganisms which are isolated from patients with diabetic foot ulcer (DFU) were reported as *Pseudomonas aeruginosa*, *Staphylococcus aureus*, *Escherichia coli*, *Enterococcus* spp., *Streptococcus* spp., *Proteus mirabilis* and anaerobes[11]. Among them, *S. aureus* and *P. aeruginosa* are the major cause of DFIs. For instance, polymicrobial (mixed microbial culture) *S. aureus* and *P. aeruginosa* infections appear frequently in deep or chronic wounds[12,13]. The mutualistic and parasitic interactions cause synergistic association among the two species which led to the development of infections[14,15]. Inclusion of mixed microbial species in a single community of biofilms causes several benefits, such as an enlarged gene pool with more effectual DNA sharing,

[1]Medical Microbiology and Molecular Biology Lab., Interdisciplinary Biotechnology Unit, Aligarh Muslim University, Aligarh 202002, UP, India. [2]Department of Biochemical Engineering and Biotechnology, Indian Institute of Technology , Delhi, India. [3]Department of Pathology, JNMC, A.M.U., Aligarh, India. [4]Department of Biochemistry, F/O Medicine, JNMC, A.M.U., Aligarh, India. ✉email: asadukhan72@gmail.com

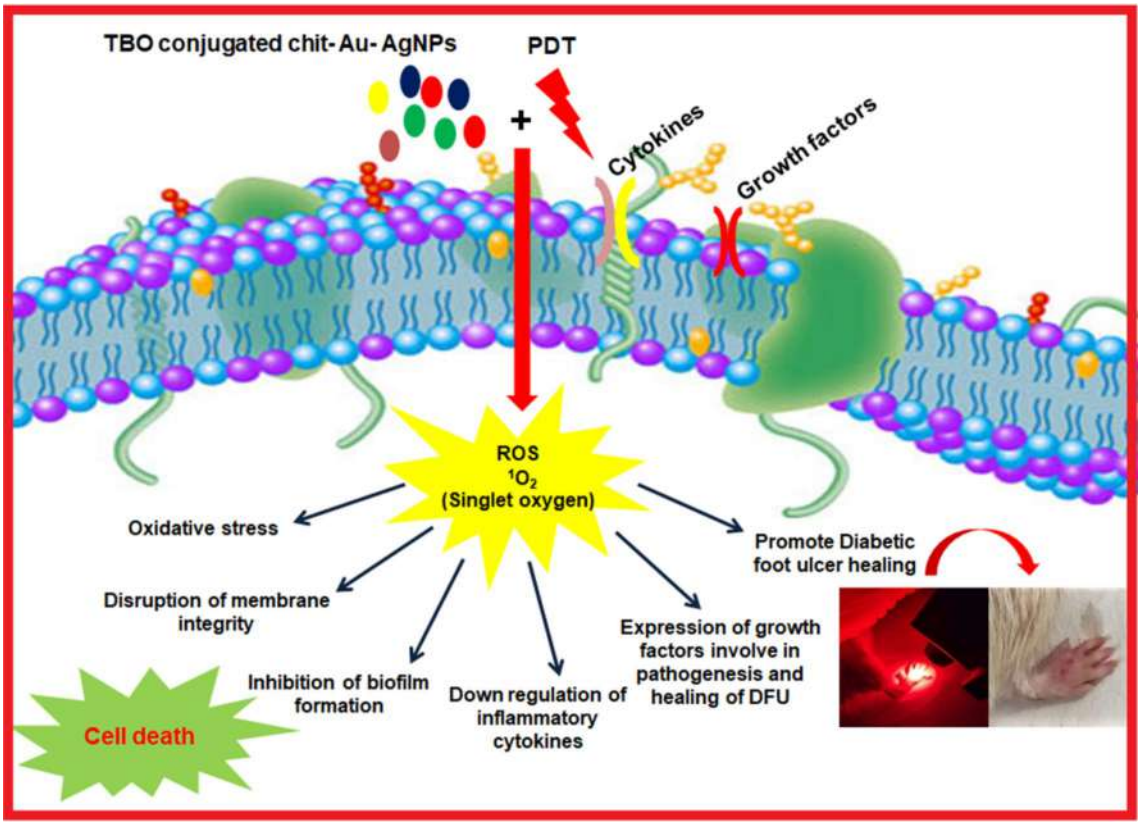


**Figure 1.** Schematic representation of nanoparticle mediated antimicrobial photodynamic therapy against diabetic foot ulcer.

quorum sensing systems, metabolic cooperation, etc[16]. Since no antibiotic is left to treat such infections therefore, the need of an hour is to search for alternative therapy.

Metallic nanomaterials have attracted considerable attention to control the spread of infections over the last decade. These nanomaterials in different forms may bind to the cell surface of bacteria, causing membrane damage which in turn leads to an alteration in membrane potential as well as permeability followed by cytoplasmic leakage and cellular damage. In addition, metal nanoparticles produce different kinds of intracellular reactive oxygen species (ROS) which damages microbial membrane and other cellular components, thereby causing cell death[17–19]. The antimicrobial actions of metal nanoparticles including gold and silver have already been established. Gold nanoparticles (AuNPs) have been reported to be used extensively in therapeutics and diagnosis because of their small size and large surface-area-to-volume ratio[20–22]. Here, we initiated to fabricate a chitosan-coated gold nanoparticle (chit-AuNPs) as a core material[23], followed by the deposition of the silver shell. It is worth to mention that chitosan biopolymer act as an effective reducing and stabilizing agent as well as an external layer to provide the nanocomposites with several advantages[24]. Whereas, silver ions act upon various sites in microorganisms to cease their growth. Previously, it was shown that silver nanoparticles are generally liable for the contact killing of microorganisms[25–30]. In this regard, chitosan coated gold–silver core–shell nanoparticles (chit–Au–AgNPs) would be an efficient antimicrobial agent. Moreover, we intend to conjugate chit-Au–AgNPs metal composite with a photosensitizer (TBO), which will further enhance the antibacterial efficacy of this nanocomposite and possibly eradicates infection caused by resistant bacteria. Toluidine blue O (TBO) is a cationic phenothiazine dye that has been well studied as an antibacterial photosensitizer. It departs a high quantum of cytotoxic singlet oxygen during photosensitization with 630 nm wavelength of light[31–36]. Recently, photodynamic therapy (PDT) has proven as multipronged strategy, which is far most effective to inactivate microorganisms such as bacteria, fungi, viruses and yeast[37–48], as compared to antibiotics. PDT combines the action of light on a non-toxic photosensitizer (PS) which causes production of reactive oxygen species being toxic to cellular components. This approach is highly effective in killing MDR strains since microorganisms do not acquire resistance toward PDT[49].The use of TBO–chit–Au–AgNPs mediated PDT has not been reported yet. Therefore, we initiated this study to provide a novel approach toward potential applications of nano-phototheranostic complex, as a nontoxic antibacterial agent to combat DFU caused by multi-drug resistant bacterial strains (Fig. 1).

## Results

**Synthesis and characterization of TBO–chit–Au–AgNPs.** Chitosan–coated gold nanoparticles (chit–AuNPs, Fig. 2A(a)) were synthesized as core materials instead of citrate or dextran capped gold nanoparticles to produce biocompatible gold–silver core–shell nanoparticles (chit–Au–AgNPs). The synthesized

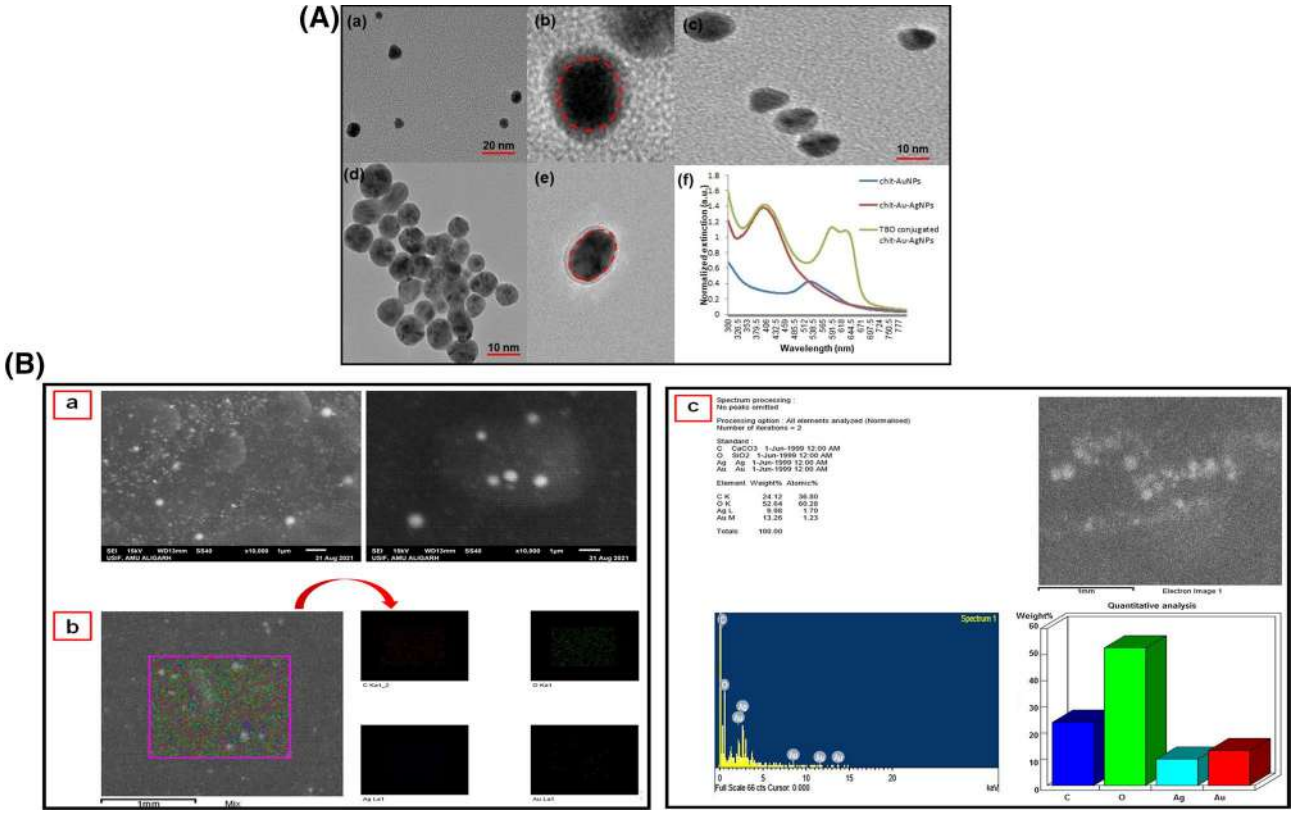


**Figure 2.** Characterization of nanoparticles: (**A**) (a) TEM image of spherical chit–AuNPs. (b)–(d) TEM images of chit–Au–AgNPs after additions of $AgNO_3$ aliquots. The interface between the Au–core and the Ag–shell was marked by a red dashed line in (**A**(b)). (e) A closer view of an Au–AgNP coated by a chitosan layer. (f) UV–Vis absorption spectra of chit–AuNPs, chit–Au–AgNPs and TBO–chit–Au–AgNPs. (**B**) (a) Scanning electron microscopy (SEM) images of chit–Au–AgNPs, (b) Elemental distribution of Au, Ag, C and O in the sample (chit–Au–AgNPs) from Energy dispersive X-ray spectrometry (EDS) analysis, (c) EDS profile of chit–Au–AgNPs and quantitative analysis of Au, Ag, C and O in the sample.

TBO–chit–Au–AgNPs were characterized by UV-spectroscopy, TEM, DLS and Zeta potential. Furthermore, we have performed elemental mapping of chit–Au–AgNPs using scanning electron microscopy (SEM) with energy dispersive X-ray spectrometry (EDS). The addition of TBO with chit–Au–AgNPs under dark conditions has led to the formation of TBO–chit–Au–AgNPs (Fig. 2A(f)-green spectrum). The UV-visible spectrum of the synthesized chit–AuNPs (Fig. 2A(f)-blue spectrum) exhibits a well-defined SPR (surface plasmon resonance) band centered at 530 nm. Thereafter, $AgNO_3$ aliquots were added into a solution containing colloidal chit-AuNPs and ascorbic acid, changes the SPR extinction spectrum. For instance, after 60 min, occurrence of a new band takes place at 405 nm (Fig. 2A(f)-red spectrum) upon first addition of $AgNO_3$ aliquots. The morphological progression of chit–Au–AgNPs was further confirmed by TEM. The dark gold core and the brighter silver shell as observed in Fig. 2A(b–d), was clearly distinguishable because of higher electronic density of gold than silver. Absence of free AgNPs in TEM images illustrated the stepwise addition of $AgNO_3$, leading to the formation of bimetallic nanoparticles than monometallic. Furthermore, Fig. 2A(e) showed the presence of chitosan layer as a faint shadow which encapsulates the Au–AgNPs after their formation. Moreover, the result of scanning electron microscopy (SEM) with energy dispersive X-ray spectrometry (EDS) analysis (EDX) clearly showed the presence of Au, Ag and chitosan in pure form with weights of 13.26% Au, 9.98% Ag, 24.12% C and 52.64% O in the sample (Fig. 2B-a, b and c).The average size of chit–AuNPs, chit–Au–AgNPs and TBO–chit–Au–AgNPs were found to be 129.4 nm, 131 nm, and 134 nm, respectively, as analyzed by dynamic light scattering (DLS) (Table 1). Changes in the polydispersity index (PDI) were also measured over this time. The PDI of chit-AuNPs, chit–Au–AgNPs and TBO–chit–Au–AgNPs remained low, indicating that there is least or no aggregation of particles. In addition, the result of zeta potential clearly illustrates chit–Au–AgNPs synthesized through stepwise addition of $AgNO_3$ retains their positive zeta potential of +37.6 mV, which shows that the polymeric coating is well-preserved all through the formation of core–shell nanoparticles (chit–Au–AgNPs). Even after the addition of TBO, chit–Au–AgNPs exhibited strong positive zeta potential of +41.2 mV, suggesting the stability and biocompatibility of synthesized TBO–chit–Au–AgNPs (Table 1).

**Effect of TBO–chit–Au–AgNPs mediated photodynamic therapy on cellular toxicity.** The relative cellular viability of L929 fibroblast cells in the presence of various concentrations (0.25 mM, 0.5 mM and 1 mM) of TBO–chit–Au–AgNPs with and without laser irradiation is shown in Fig. 3. Almost 65.12% and

| Sample | Size (d, nm) | Polydispersity index (PDI) | Zeta potential (mV) |
|---|---|---|---|
| Chit–AuNPs | 129.4 | 0.107 | 49 |
| Chit–Au–AgNPs | 131 | 0.067 | 37.6 |
| TBO–chit–Au–AgNPs | 134 | 0.085 | 41.2 |

**Table 1.** Hydrodynamic diameter (size by number) obtained from DLS, Polydispersity index (PDI) and zeta potential values of chit–AuNPs, chit–Au–AgNPs and TBO–chit–Au–AgNPs.

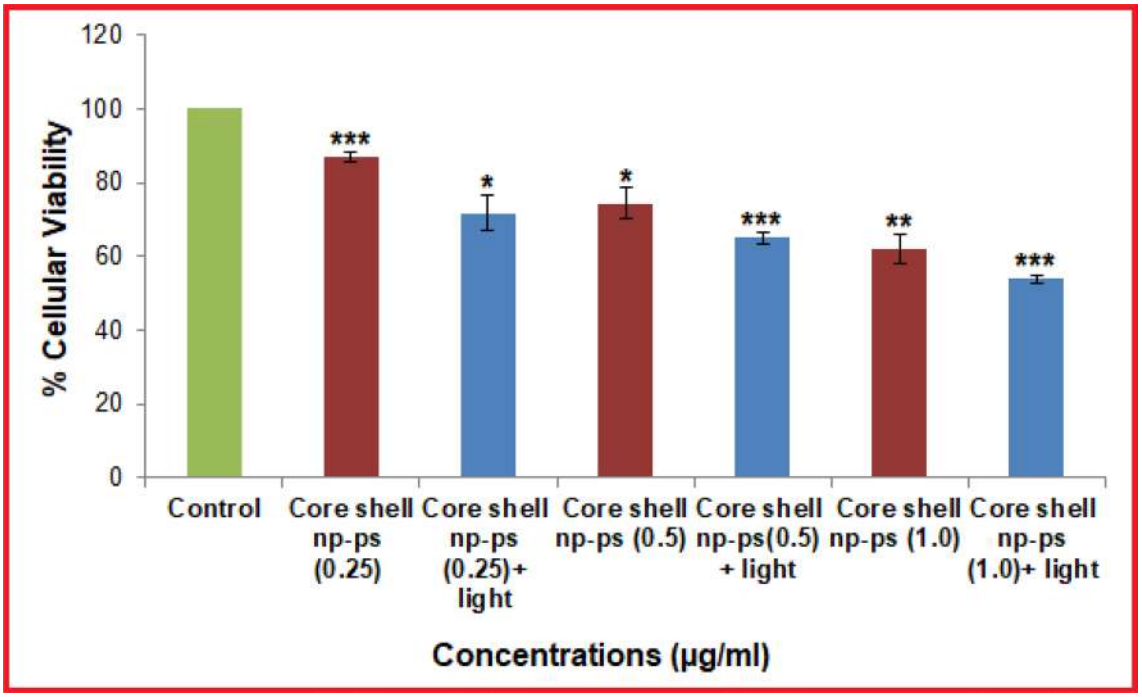


**Figure 3.** Cytotoxicity assay: Percentage viable cells as measured after 24 h, after treatment with TBO–chit–Au–AgNPs in absence and presence of laser irradiation. Data expressed as mean ± SD, n = 3 ($p$-value $^{*}p < 0.01$; $^{**}p < 0.001$, $^{***}p < 0.0001$, ns = not significant).

74.32% viability were observed at our tested concentration (0.5 mM) with and without laser irradiation respectively. Thus, the concentration of the TBO–chit–Au–AgNPs and exposure time (100 J/cm$^2$) of red laser light used in this study was found to be non-toxic.

**In vitro anti-bacterial activity of TBO–chit–Au–AgNPs mediated photodynamic therapy on monomicrobial and polymicrobial biofilms of *S. aureus* and *P. aeruginosa*.** The antibacterial activity of TBO–chit–Au–AgNPs in the presence as well as in the absence of laser irradiation was assessed using colony formation assay against polymicrobial biofilms and compared with that of monomicrobial biofilms. After incubation for 24 h, the resulting monomicrobial biofilms showed 2.76 $\log_{10}$ CFU/mL reduction of *S.aureus* and 2.17 $\log_{10}$ CFU/mL reduction of *P. aeruginosa* in the group treated with TBO–chit–Au–AgNPs only. While, 2.15 $\log_{10}$ CFU/mL reduction was seen in polymicrobial biofilms (Fig. 4). A substantial reduction in bacterial load was achieved when monomicrobial and polymicrobial biofilms of *S. aureus* and *P. aeruginosa* treated with TBO–chit–Au–AgNPs and subsequently to 100 J/cm$^2$ of laser irradiation. A 6.86 $\log_{10}$ CFU/mL and 5.4 $\log_{10}$ CFU/mL reduction was found in the monomicrobial biofilm of *S. aureus* and *P. aeruginosa*, respectively, whereas 5.31 $\log_{10}$ CFU/mL reductions were observed in the polymicrobial biofilms of both the species (Fig. 4). The bacterial load reduction in the polymicrobial biofilms of *S. aureus* and *P. aeruginosa* was found to be lower than monomicrobial biofilms of both the species after nano-photodynamic therapy (Supplementary Fig. S1).

**Generation of reactive oxygen species and singlet oxygen quantification.** Our data showed increase production of intracellular ROS in TBO–chit–Au–AgNPs mediated photodynamic therapy treated group as compared to TBO–chit–Au–AgNPs alone, both in monomicrobial as well as in polymicrobial biofilms. Whereas, no significant ROS production was seen in the group treated with only light. Therefore, we have not selected only light treated group for further studies. Thus, we conclude that the potentiation of killing or enhanced antibacterial activity is dependent upon the generation of ROS (Fig. 5a–c). However, the photoinac-

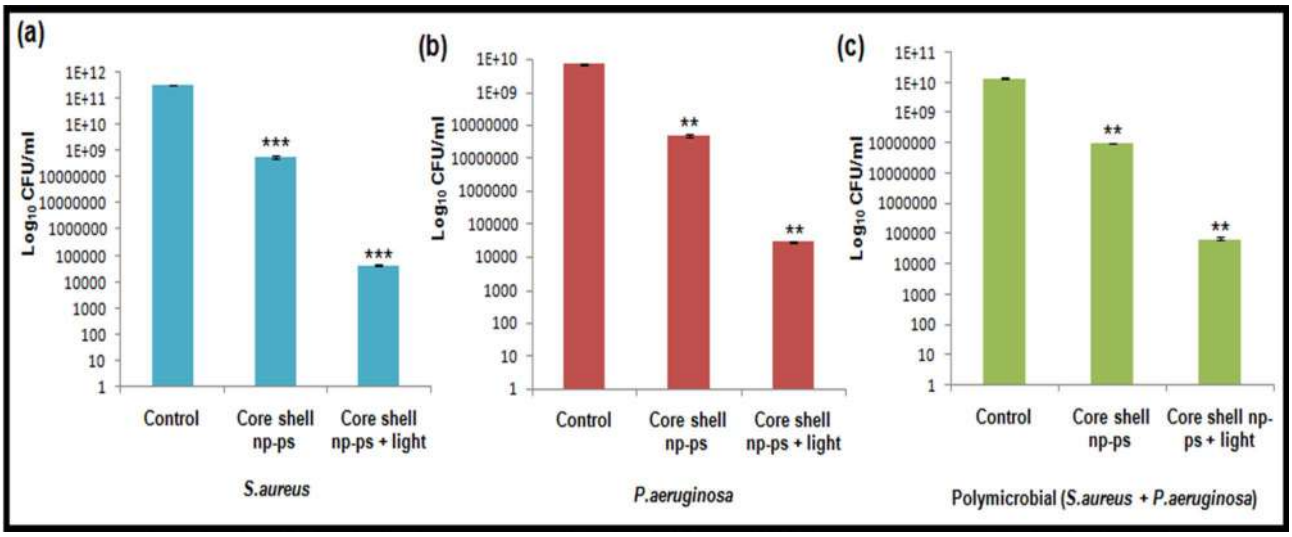


**Figure 4.** In vitro colony formation: (**a**) Monomicrobial *S. aureus*, (**b**) Monomicrobial *P. aeruginosa* and, (**c**) Polymicrobial *S. aureus* + *P. aeruginosa* colonies after incubation with TBO–chit–Au–AgNPs, TBO–chit–Au–AgNPs followed by irradiation with 630 nm laser for 12 min and 50 s which corresponds to 100 J/cm$^2$ at 0.1300 W/cm$^2$. Data are presented as mean ± SD (n = 3) and normalized to that of untreated control. Three replicates were performed for each experiment. Statistical significance was determined using one-way analysis of variance ($p$-value $^*p < 0.01$, $^{**}p < 0.001$, $^{***}p < 0.0001$, ns = not significant).

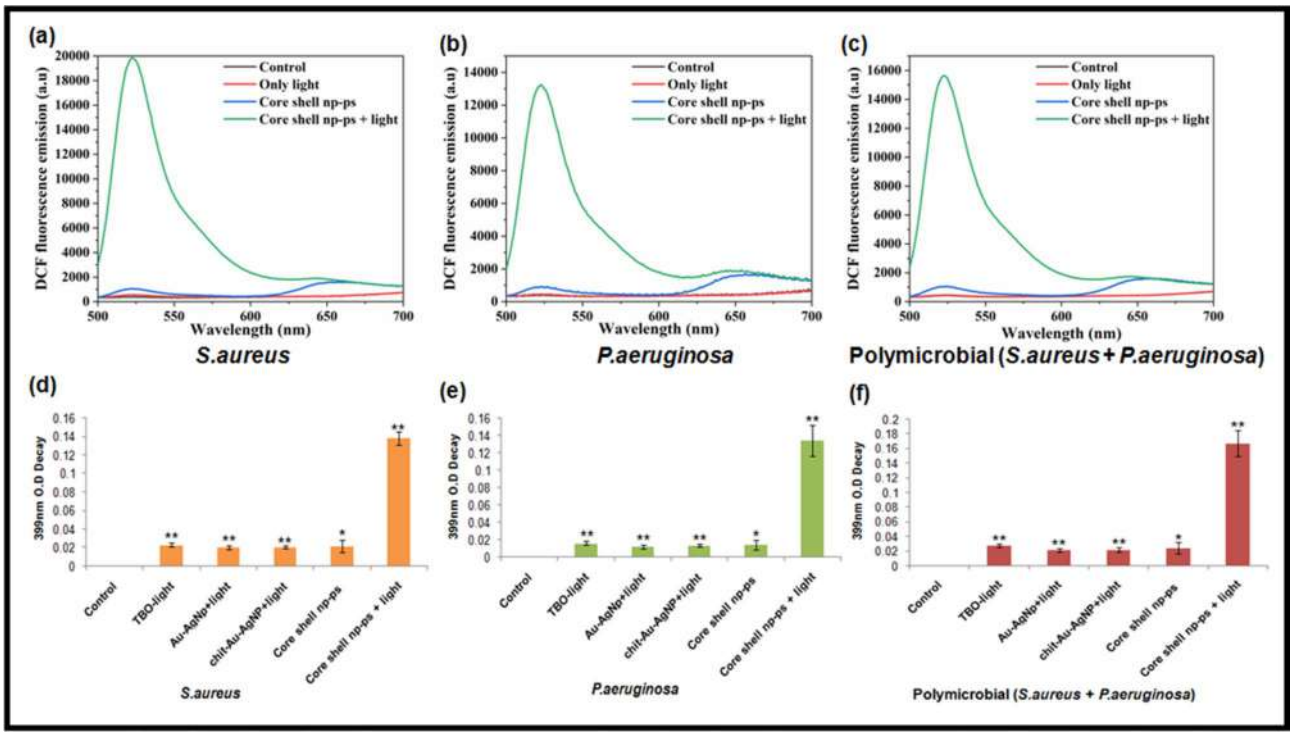


**Figure 5.** Detection of total reactive oxygen species (**a**)–(**c**) and quantification of singlet oxygen (**d**)–(**f**) in monomicrobial *S. aureus*, monomicrobial *P. aeruginosa* and polymicrobial *S. aureus* + *P. aeruginosa* biofilms in control group, TBO–chit–Au–AgNPs treated group and TBO–chit–Au–AgNPs + laser treated group. 630 nm laser (100 J/cm$^2$, 12 min and 50 s) were used in the corresponding laser group. The data represents an average of triplicate experiments ± SD ($p$-value $^*p < 0.01$, $^{**}p < 0.001$, $^{***}p < 0.0001$, ns = not significant).

tivation was found to be more pronounced in monomicrobial biofilm than polymicrobial biofilms of both the species.

Furthermore, to confirm the type of phototoxicity, we have measured the degradation rate of AMDA. Since, the amount of ROS produced is directly proportional to the bacterial cell death; our data revealed enhanced production of $^1O_2$ in TBO–chit–Au–AgNPs mediated PDT treated group as compared to control and only

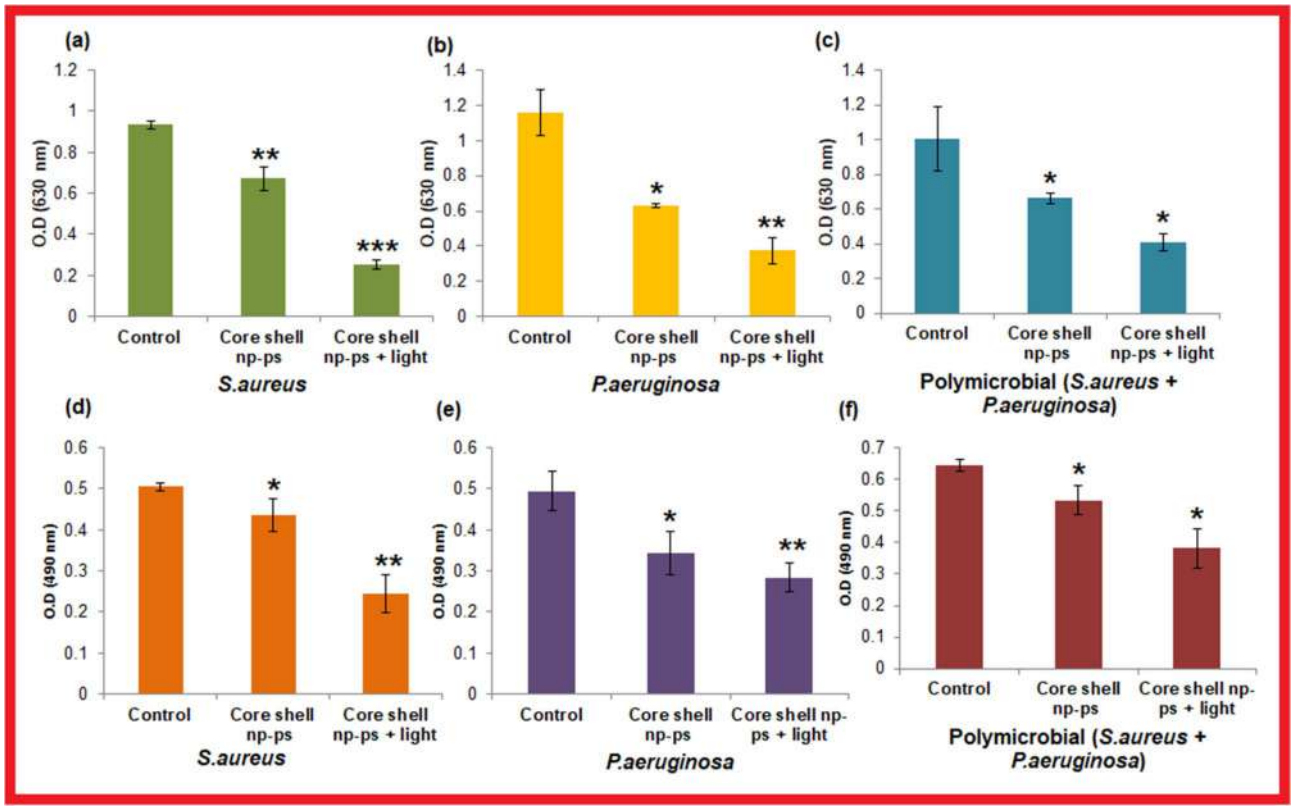


**Figure 6.** Antibiofilm forming ability of TBO–chit–Au–AgNPs mediated photodynamic therapy: (**a**)–(**c**) represents inhibitory effect of TBO–chit–Au–AgNPs mediated PDT on monomicrobial *S. aureus*, monomicrobial *P. aeruginosa* and polymicrobial *S. aureus* + *P. aeruginosa* biofilms, respectively as quantified by Crystal violet assay. Absorbance was measured at 630 nm. Figure (**d**)–(**f**) showed effect of TBO–chit–Au–AgNPs mediated PDT on extracellular polysaccharide substance (EPS) reduction as quantified by Congo-red assay. Absorbance was measured at 490 nm. The data represent an average of triplicate experiments ± SD. (*p*-value $^{*}p < 0.01$, $^{**}p < 0.001$, $^{***}p < 0.0001$, ns = not significant).

TBO–chit–Au–AgNPs treated groups (Fig. 5d–f). This confirmed that type II photochemistry is the major photochemical reaction involved in TBO–chit–Au–AgNPs mediated photodynamic therapy on monomicrobial and polymicrobial biofilms of *S. aureus* and *P. aeruginosa*.

**Anti-biofilm effect of TBO–chit–Au–AgNPs mediated photodynamic therapy.** The result of crystal violet assay showed 28.02% and 34.04% reduction in the monomicrobial *S. arureus* and *P. aeruginosa* biofilm formation, respectively, after treatment with, exclusively TBO–chit–Au–AgNPs, whereas 45.89% of polymicrobial biofilms were found to be reduced. Moreover, significant decrease in microbial biomasses was found in TBO–chit–Au–AgNPs mediated photodynamic therapy treated group as compared to control and exclusively TBO–chit–Au–AgNPs treated groups. Our data showed 72.82% and 59.15% reduction in the monomicrobial biofilm of *S. aureus* and *P. aeruginosa,* respectively, while 67.69% reduction was found in the polymicrobial biofilms after treatment with TBO–chit–Au–AgNPs and subsequently to 100 J/cm$^2$ of laser irradiation (Fig. 6a–c; Tables S1, S2). Besides this, EPS production was reduced by 13.65% and 30.71% in monomicrobial biofilm of *S. aureus* and *P. aeruginosa* whereas 17.16% in polymicrobial biofilms after being treated with exclusively TBO–chit–Au–AgNPs. While, 51.55% and 42.71% EPS reduction was achieved in monomicrobial biofilm of *S. aureus* and *P. aeruginosa,* respectively, after being photoinactivated by TBO–chit–Au–AgNPs. However, 40.9% reduction was seen in polymicrobial biofilms as shown in Fig. 6d–f.

**Visualization of biofilms architect after TBO–chit–Au–AgNPs mediated photodynamic therapy.** Confocal and scanning electron microscopy was performed to examine the morphological changes in bacteria after TBO–chit–Au–AgNPs mediated photodynamic therapy, and to elucidate the underlying antibacterial mechanisms. CLSM micrographs illustrate greater disruption of polymicrobial biofilms of *S. aureus* and *P. aeruginosa* in TBO–chit–Au–AgNPs mediated photodynamic therapy treated group (Fig. 7i) as compared to control (Fig. 7c) and exclusively TBO–chit–Au–AgNPs (Fig. 7f). Moreover, the monomicrobial biofilms of *S. aureus* and *P. aeruginosa* was more severely disrupted, almost all the bacterial cells in the biofilms were found dead in TBO–chit–Au–AgNPs mediated PDT group (Fig. 7g, h), as compared to control (Fig. 7a, b) and exclusively TBO–chit–Au–AgNPs treated group (Fig. 7d, e). Thereby, demonstrating strong antibiofilm action of TBO–chit–Au–AgNPs mediated photodynamic therapy. Furthermore, the thickness of the biofilm was

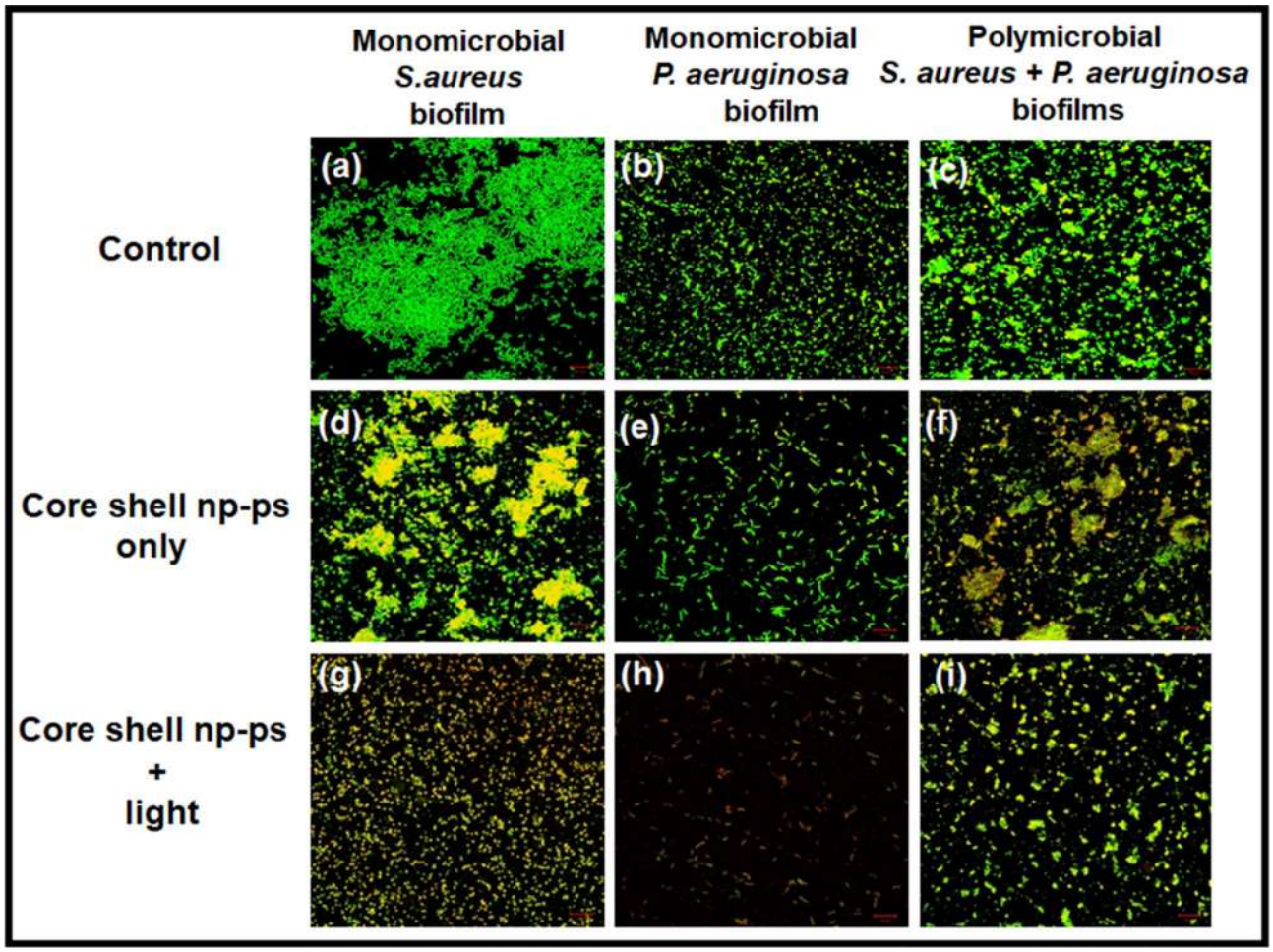


**Figure 7.** Fluorescence-based live/dead analysis of monomicrobial *S. aureus*, monomicrobial *P. aeruginosa* and polymicrobial *S. aureus* + *P. aeruginosa* biofilms: Representative fluorescence images of SYTO 9 (live, green) and PI (dead, red) stained bacteria in the groups of control (**a**)–(**c**), TBO–chit–Au–AgNPstreated (**d**)–(**f**) and TBO–chit–Au–AgNPs + laser treated (**g**)–(**i**). 630 nm laser (100 J/cm$^2$, 12 min and 50 s) were used in the corresponding laser group. Scale bar = 10 µm.

also recorded (Supplementary Fig. S2). TBO–chit–Au–AgNPs treatment reduced the thickness of the biofilm to approximately 4 µm and 3 µm in monomicrobial biofilm of *S. aureus* and *P. aeruginosa,* respectively, as compared to control (6 µm and 4 µm, respectively). However, the thickness was found to be 2.5 µm and 2 µm, respectively in TBO–chit–Au–AgNPs mediated PDT treated group, suggesting prevalence of dead cells throughout the biofilm. Likewise, polymicrobial biofilm of *S. aureus* and *P. aeruginosa* treated with TBO–chit–Au–AgNPs mediated PDT decreases the thickness of the biofilm to approximately 3 µm as compared to control (8 µm) and TBO–chit–Au–AgNPs (6 µm).This observation was further supported by the scanning electron microscopy. The control groups of monomicrobial as well as polymicrobial *S. aureus* and *P. aeruginosa* biofilms displayed highly dense and compact microbial cells (Fig. 8a–c). While, after treatment with TBO–chit–Au–AgNPs followed by exposure to 100 J/cm$^2$ of laser light, the density of the microbial cells in the monomicrobial as well as in the polymicrobial biofilms of both the species decreases significantly (Fig. 8g–i). Less reduction was observed in only TBO–chit–Au–AgNPs treated groups (Fig. 8d–f). Furthermore, TBO–chit–Au–AgNPs mediated PDT treated groups showed detrimental effects on cell wall with significant dispersion of the cells leading to leakage of the cellular content, thus obliterating the structural integrity of the biofilm.

**In vivo efficacy of TBO–chit–Au–AgNPs mediated photodynamic therapy in the treatment of Diabetic Foot Ulcer.** The efficacy of TBO–chit–Au–AgNPs mediated photodynamic therapy in healing of diabetic foot ulcer in male wistar rats was checked. Streptozotocin (STZ)-induced type 2 DM rats with blood glucose level higher than 300 mg/dl were developed and used for further study (Table 2). Change in weight of the rats during the course of the experiment were also monitored (Table S3). Our result showed that daily topical exposure of TBO–chit–Au–AgNPs followed by light irradiation led to the marked reduction of *S. aureus* and *P. aeruginosa* colonization in diabetic foot ulcer rats within 7 days, starting from the day 3 post infection (Figs. 9, 10A–C, Table S4). Furthermore, histopathological analysis of untreated monomicrobial and polymicrobial DFU (Fig. 11B-d–f) revealed dense population of inflammatory cells with focal neutrophilic infiltrate attached to the stratified squamous epithelium as compared to control, diabetic (Fig. 11A) and ulcerated groups (Fig. 11B-

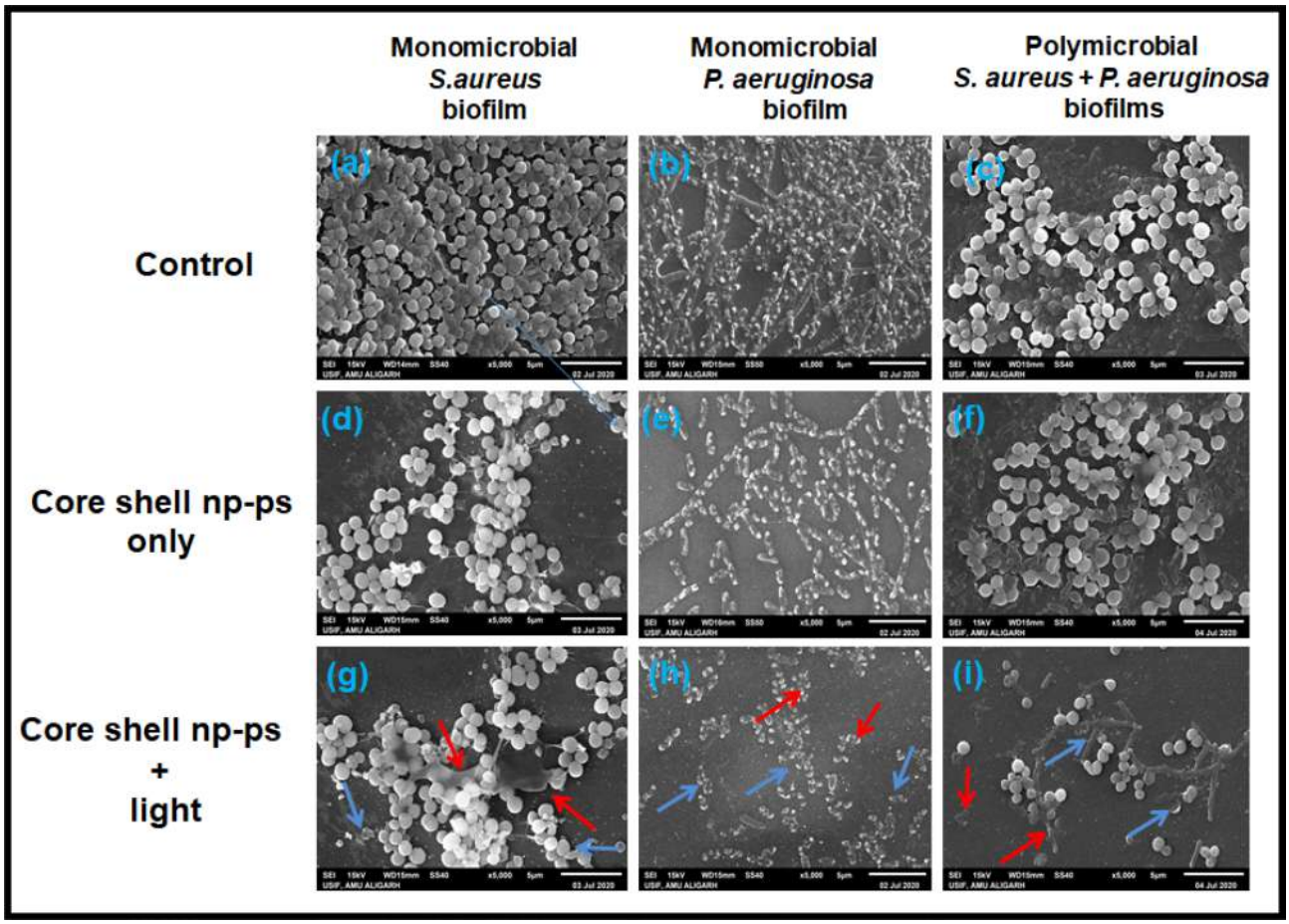


**Figure 8.** Scanning electron microscopy (SEM) images of monomicrobial *S.aureus*, monomicrobial *P. aeruginosa* and polymicrobial *S. aureus* + *P. aeruginosa* biofims of control (**a**)–(**c**), TBO–chit–Au–AgNPs treated (**d**)–(**f**) and TBO–chit–Au–AgNPs + laser treated (**g**)–(**i**). 630 nm laser (100 J/cm$^2$, 12 min and 50 s) were used in the corresponding laser group. Red arrow indicates bursting and release of cellular constituents while blue arrow indicates complete rupturing of the cells.

a–c). In addition, the ulcerated squamous epithelium in untreated DFU rats showed decrease collagenization with few basal thin capillaries and mild fibrosis. This confirms the incidence of an ongoing infection. However, the ulcer sites of the TBO–chit–Au–AgNPs treated group showed acanthotic (thickened) squamous epithelium with moderate fibrosis. Besides this, restorative ulcer was observed with focal moderately thick collagen fibers and few compressed capillaries (Fig. 11B-g–i). In comparison, TBO–chit–Au–AgNPs mediated photodynamic therapy treated DFU showed intact stratified squamous epithelium with marked neo-angiogenesis and collagenization (Fig. 11B-j–l).

**Effect of TBO–chit–Au–AgNPs mediated photodynamic therapy on growth factors and inflammatory cytokines in diabetic foot ulcer development and healing.** The expression levels of growth factors and cytokines in control (normal) rats were compared with diabetic and non-diabetic rats with healed (treated) and unhealed (untreated) ulcers.

We have found that failure of an ulcer to heal in diabetic rats was linked with an increased level of pro-inflammatory cytokines, such as IL-6 and TNF-α. Furthermore, the expression levels of pro-inflammatory cytokines were significantly higher in DFU rats with polymicrobial infections as compared to DFU rats with monomicrobial infection. However, decreased levels of these cytokines were found in TBO–chit–Au–AgNPs mediated photodynamic therapy treated groups as compared to control, untreated and only TBO–chit–Au–AgNPs treated groups, implying restoration of immunosuppression (Fig. 12-a, b). In addition, our data demonstrated significantly higher levels of EGF and VEGF in all those groups of rats whose ulcers healed as compared to those groups whose ulcers did not healed (Fig. 12-c, d). However, their expression level was found to be lower in DFU rats with polymicrobial infections than that of monomicrobial infection, as the severity of infection was found to be more in polymicrobial state of infection. Besides this, elevated level of TGF-β-1 was found in all diabetic groups (with and without foot ulcer) (Fig. 12e). Moreover, we have found expression levels of TGF-β-1 were significantly higher in diabetic rats with polymicrobial infections as compared to monomicrobial infection. In addition, IGF-1 level was found to be lower in diabetic rats as compared to non-diabetic and control rats. However, considerable decrease was found in DFU rats with polymicrobial infections (Fig. 12f). Hence, the data

| S. no. | Groups | Blood sugar concentration (mg/dL) in overnight fasting rats before the injection of Streptozotocin (STZ) | Blood sugar concentration (mg/dL) after the injection of Streptozotocin (STZ) |
|---|---|---|---|
| 1 | Control (normal rats) | i. 102<br>ii. 92<br>iii. 87<br>iv. 108 | – |
| 2 | Diabetic without ulcer (untreated rats) | i. 98<br>ii. 90<br>iii. 89<br>iv. 99 | i'. 368<br>ii'. 239<br>iii'. 366<br>iv'. 261 |
| 3 | *Pseudomonas aeruginosa*<br>Diabetic with ulcer (untreated rats) | i. 110<br>ii. 102<br>iii. 94<br>iv. 87 | i'. 325<br>ii'. 338<br>iii'. 302<br>iv'. 319 |
| 4 | *Pseudomonas aeruginosa*<br>Diabetic with ulcer (TBO–chit–Au–AgNPs treated rats) | i. 95<br>ii. 130<br>iii. 94<br>iv. 102 | i'. 380<br>ii'. 397<br>iii'. 394<br>iv'. 382 |
| 5 | *Pseudomonas aeruginosa*<br>Diabetic with ulcer (TBO–chit–Au–AgNPs + light treated rats) | i. 108<br>ii. 100<br>iii. 80<br>iv. 98 | i'. 376<br>ii'. 265<br>iii'. 277<br>iv'. 264 |
| 6 | *Staphylococcus aureus*<br>Diabetic with ulcer (untreated rats) | i. 138<br>ii. 112<br>iii. 98<br>iv. 104 | i'. 309<br>ii'. 386<br>iii'. 287<br>iv'. 312 |
| 7 | *Staphylococcus aureus*<br>Diabetic with ulcer (TBO–chit–Au–AgNPs treated rats) | i. 139<br>ii. 87<br>iii. 94<br>iv. 93 | i'. 299<br>ii'. 310<br>iii'. 264<br>iv'. 317 |
| 8 | *Staphylococcus aureus*<br>Diabetic with ulcer (TBO–chit–Au–AgNPs + light treated rats) | i. 130<br>ii. 123<br>iii. 117<br>iv. 103 | i'. 385<br>ii'. 305<br>iii'. 377<br>iv'. 338 |
| 9 | Polymicrobial (*Staphylococcus aureus* + *Pseudomonas aeruginosa*)<br>Diabetic with ulcer (untreated rats) | i. 104<br>ii. 110<br>iii. 96<br>iv. 117 | i'. 291<br>ii'. 271<br>iii'. 359<br>iv'. 331 |
| 10 | Polymicrobial (*Staphylococcus aureus* + *Pseudomonas aeruginosa*)<br>Diabetic with ulcer (TBO–chit–Au–AgNPs treated rats) | i. 109<br>ii. 106<br>iii. 103<br>iv. 122 | i'. 362<br>ii'. 358<br>iii'. 376<br>iv'. 321 |
| 11 | Polymicrobial (*Staphylococcus aureus* + *Pseudomonas aeruginosa*)<br>Diabetic with ulcer (TBO–chit–Au–AgNPs + light treated rats) | i. 106<br>ii. 114<br>iii. 73<br>iv. 111 | i'. 319<br>ii'. 375<br>iii'. 332<br>iv'. 345 |

**Table 2.** Experimental induction of type-2 diabetes by streptozotocin (STZ) injection.

suggest that TBO–chit–Au–AgNPs mediated PDT promotes healing in DFU rats through significantly reducing cytokine production while elevating EGF and VEGF levels by regulating the expression of TGF-β-1 and IGF-1.

## Discussion

Type 2 diabetes mellitus (DM) has become an utmost health concern which comprised of 90–95% diabetes among worldwide population[1]. It has also been reported that up to one-third of people with diabetes may develop foot ulcer during their lifetime and over 50% of these ulcers become infected. This challenge is further aggravated by the emergence of multidrug-resistance (MDR) strains induced diabetic foot infections (DFIs) which leads to increasing morbidity and mortality, and risk of lower extremity amputation (LEA) which causes low quality of life[3–6]. Majority of these infections are now being caused by *Pseudomonas aeruginosa*, *Staphylococcus aureus*, *Escherichia coli*, *Enterococcus* spp., *Streptococcus* spp., *Proteus mirabilis* and anaerobes[11].

*S. aureus* and *P. aeruginosa* are two versatile bacterial pathogens that are frequently found together in chronic wound infections[12,50]. Polymicrobial (mixed microbial culture) *S. aureus* and *P. aeruginosa* infections are more virulent and/or result in worse outcomes than the single infections caused by either species[15], leading to the formation of more resistant biofilms, which are difficult to be eradicated. For instance, biofilm-forming MDR strains are far more impervious to antimicrobials than organisms in suspension[7–9]. In this regard, nanoparticle mediated photodynamic therapy emerged as an ideal candidate to meet such requirements[51,52].

Recently, chitosan coated gold–silver core–shell nanoparticles (chit–Au–AgNPs) was developed and labeled with para-mercaptobenzoic acid (4MBA) to demonstrate their ability to perform as SERS nanotags inside of human ovarian adenocarcinoma cells (NIH: OVCAR-3) under multiple excitation wavelengths[24]. Here, chit–Au–AgNPs were used for the first time in association with TBO.

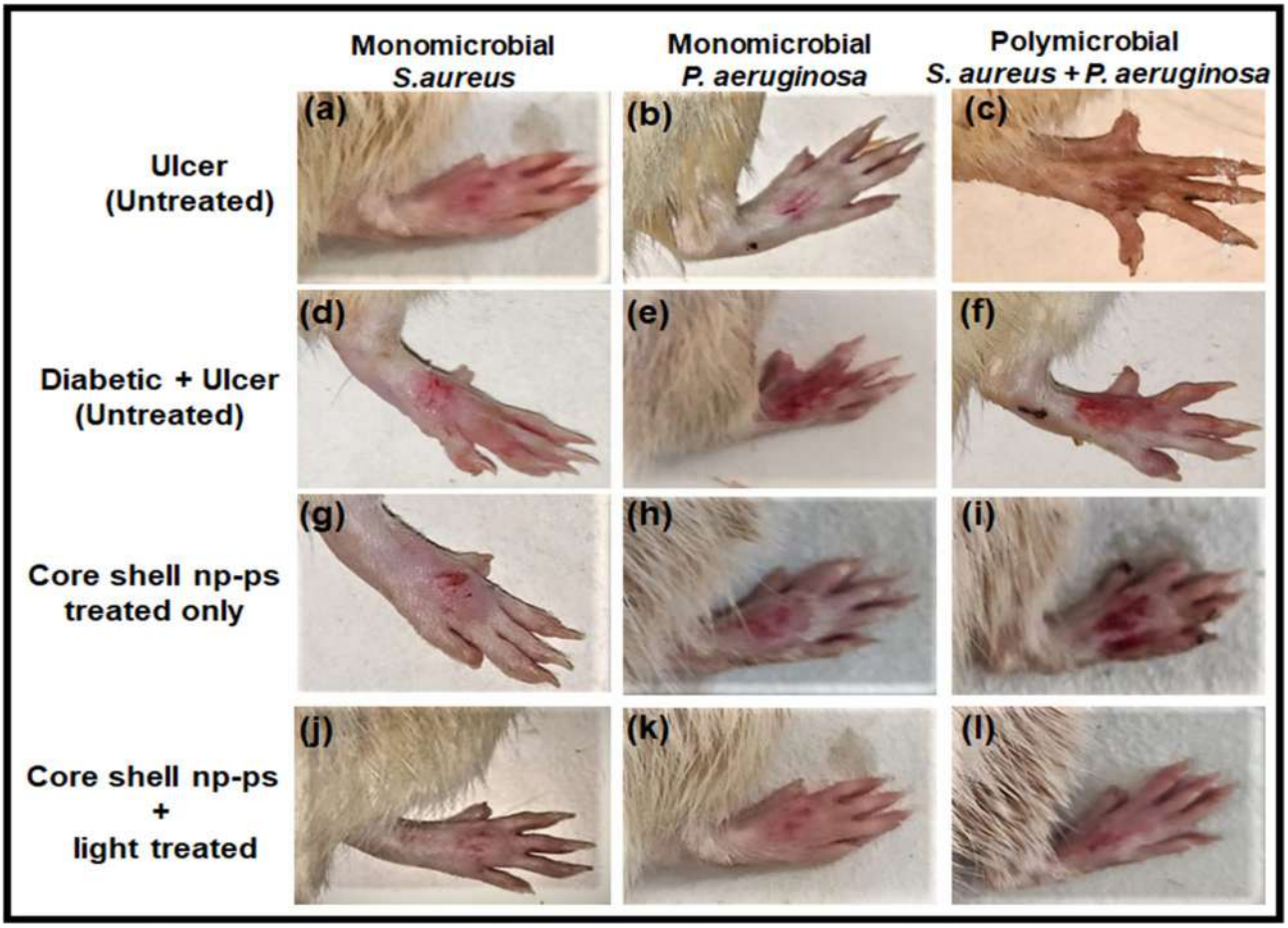


**Figure 9.** Photographic image of wistar rats: Untreated foot ulcer (**a**)–(**c**), untreated foot ulcer with diabetes (**d**)–(**f**), diabetic foot ulcer after applying TBO–chit–Au–AgNPs (**g**)–(**i**) and diabetic foot ulcer after treatment with TBO–chit–Au–AgNPs mediated PDT.

Earlier studies have shown that photosensitizer activity is significantly improved when combine with nanoparticles[49]. Our study was planned to investigate the effectiveness of novel toluidine blue conjugated gold–silver core–shell nanoparticles (TBO–chit–Au–AgNPs) mediated photodynamic therapy and demonstrate their use as a nontoxic antibacterial therapy to combat diabetic foot ulcer (DFU) caused by multi-drug resistant strains both in monomicrobial and polymicrobial state of infection.

The synthesized TBO–chit–Au–AgNPs were characterized by UV-spectroscopy, TEM, scanning electron microscopy (SEM) with energy dispersive X-ray spectrometry (EDS), DLS and Zeta potential. The UV–visible spectrum of the synthesized chit–AuNPs (Fig. 2A(f)-blue spectrum) exhibits a well-defined SPR (surface plasmon resonance) band centered at 530 nm. For instance, occurrence of a new band takes place at 405 nm (Fig. 2A(f)-red spectrum) upon first addition of $AgNO_3$ aliquots. This spectral profile has already been reported in previous studies and it confirms the successful synthesis of a thin silver layer on the surface of the gold core[53]. The morphological progression of core–shell nanoparticles (chit–Au–AgNPs) was further confirmed by TEM. The dark gold core and the brighter silver shell as observed in Fig. 2A(b–d), was clearly distinguishable because of higher electronic density of gold than silver. Furthermore, Fig. 2A(e) showed the presence of chitosan layer as a faint shadow which encapsulates the Au–AgNPs after their formation. This foremost result demonstrated not only the effective synthesis of Au–AgNPs, but also their steadiness and bio-compatibilization, which are required essentially for the use of this nanoconjugate in biological systems. We next performed elemental mapping to verify the presence of gold and silver using scanning electron microscopy (SEM) with energy dispersive X-ray spectrometry (EDS). The result confirms the formation of chit–Au–Ag nanocomposites with no additional impurities as detected in the EDS (Fig. 2B-a–c). Changes in the polydispersity index (PDI) were also measured over this time. The PDI of chit-AuNPs, chit–Au–AgNPs and TBO–chit–Au–AgNPs remained low, indicating that there is least or no aggregation of particles (Table 1). We have also measured the surface zeta potential to further confirm about the stability of nanoparticles. Our data demonstrated strong positive zeta potential of chit–Au–AgNPs (+41.2 mV) even after the addition of TBO, suggesting the stability and biocompatibility of synthesized core–shell nanoparticles (chit–Au–AgNPs) with TBO.

We next checked the cytotoxicity of TBO–chit–Au–AgNPsin the presence as well as in the absence of laser irradiation. As presented in Fig. 3, the synthesized TBO-chit–Au–AgNPs in the presence of laser irradiation did

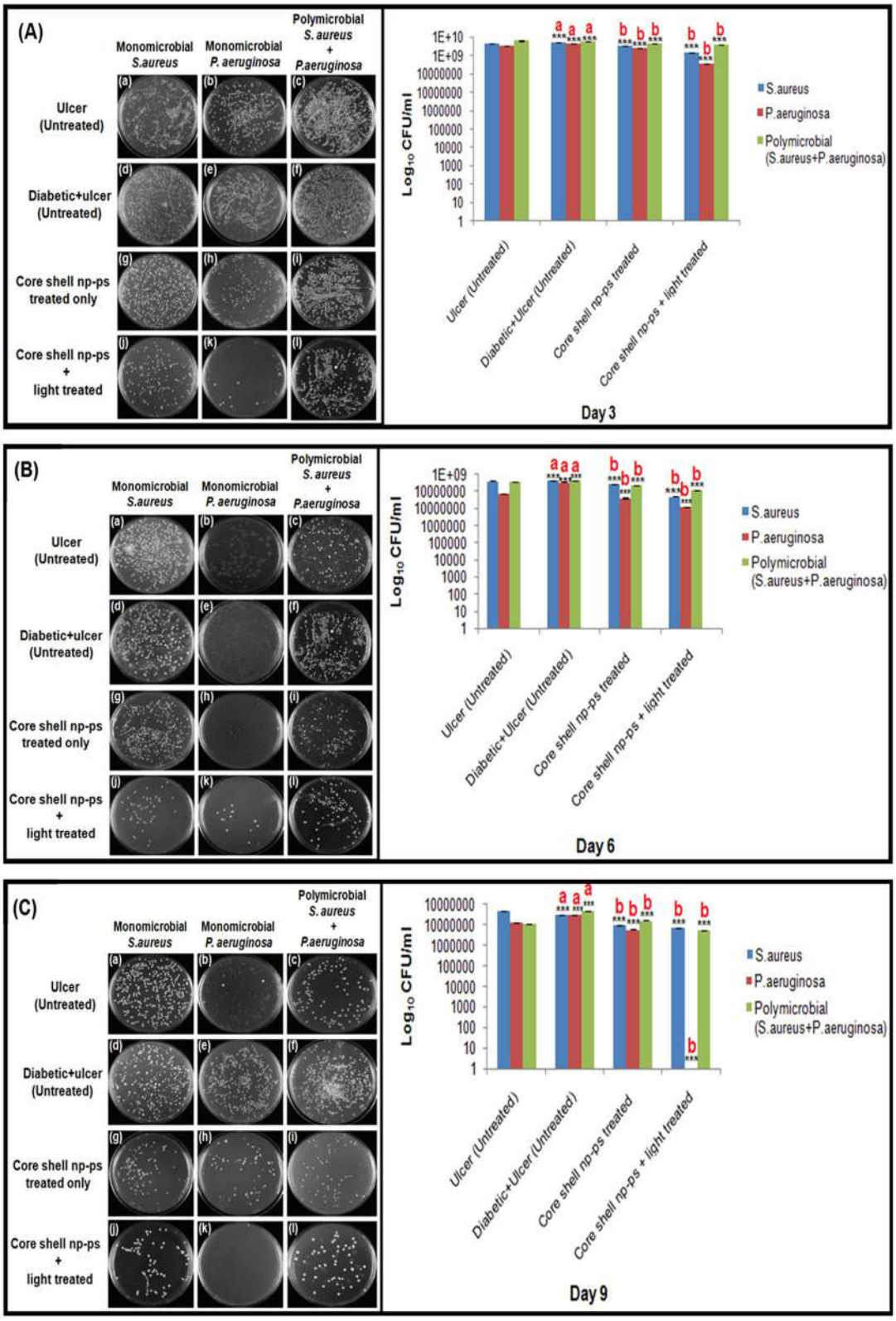


**Figure 10.** In vivo antibacterial effect of TBO–chit–Au–AgNPs mediated photodynamic therapy in DFU rats: (**A**) CFU/ml at day 3 post ulceration, (**B**) CFU/ml at day 6 post ulceration and treatment, (**C**) CFU/mL at day 9 post ulceration and treatment. Data are presented as mean ± SD (n = 4) and normalized to that of untreated control. Three replicates were performed for each experiment. Statistical significance was determined using one-way analysis of variance (*p*-value $*p < 0.01$, $**p < 0.001$, $***p < 0.0001$, ns = not significant). a—compared with untreated ulcer; b—compared with untreated diabetic foot ulcer.

not exhibit any obvious cytotoxic effects at our tested concentration (0.5 mM). This could be attributed mainly to the biological and chemical properties of chitosan, as well as low toxic effect of TBO on fibroblast cells[54,55]. Furthermore, the wavelength of red laser (630 nm) lies in the visible spectrum. Hence, the concentration of the TBO–chit–Au–AgNPs and exposure time of red laser light used in this study was found to be non-toxic.

One of the main factors responsible for the resistance of *S. aureus* and *P. aeruginosa* to both antibiotics and immune cells is their propensity to form biofilms. We therefore assessed the antibacterial activity of TBO–chit–Au–AgNPs in the presence as well as in the absence of laser irradiation using colony formation assay against polymicrobial biofilms and compared with that of monomicrobial biofilms. A substantial reduction in bacterial load was achieved when monomicrobial and polymicrobial biofilms of *S. aureus* and *P. aeruginosa* treated with TBO–chit–Au–AgNPs and subsequently to 100 J/cm$^2$ of laser irradiation (Fig. 4). The bacterial load reduction in the polymicrobial biofilms of *S. aureus* and *P. aeruginosa* was found to be lower than monomicrobial biofilms of both the species after nano-photodynamic therapy (Supplementary Fig. S1). The results from the present study illustrated synergistic interaction between *S. aureus* and *P. aeruginosa* which is in concordance with previous studies[13]. Moreover, we have found Gram-positive, *S. aureus* as more sensitive towards nanoparticle mediated photodynamic therapy as compared to Gram-negative, *P. aeruginosa*. Since, it has been reported in the literature that teichoic acid found within the cell wall of Gram-positive bacteria is the main binding site of some small molecules and nanoparticles[56]. The improved susceptibility of *S. aureus*, despite of thick peptidoglycan layer may be attributed to the interaction between positively charged TBO–chit–Au–AgNPs and the anionic teichoic acid which leads to the cleavage of the peptidoglycan layer and pore formation in the membrane.

In order to illustrate the above outcomes, we further analyzed the mechanism behind the antibacterial activity of TBO–chit–Au–AgNPs mediated photodynamic therapy using DCFH-DA and quantified the production of total reactive oxygen species (ROS) under laser irradiation. Our data showed increase production of intracellular ROS in TBO–chit–Au–AgNPs mediated photodynamic therapy treated group as compared to TBO–chit–Au–AgNPs alone, both in monomicrobial as well as in polymicrobial biofilms. However, the photoinactivation was found to be more pronounced in monomicrobial biofilm than polymicrobial biofilms of both the species. Thus, we conclude that the potentiation of killing or enhanced antibacterial activity is dependent upon the generation of ROS (Fig. 5a–c). Additionally, bacterial cells have sufficient amount of scavengers such as catalase, peroxidase and superoxide dismutase to thwart the free radical mediated bactericidal activity, however they have no remedy against the singlet oxygen molecule, as a result, $^1O_2$ leads to maximum cell damage[57]. Therefore, to confirm the type of phototoxicity, we have used AMDA. Our data revealed enhanced production of $^1O_2$ in TBO–chit–Au–AgNPs mediated PDT treated group as compared to control and only TBO–chit–Au–AgNPs treated groups (Fig. 5d–f).

Furthermore, the ability of bacterial adherence and exopolysaccharide production which are significantly important for the formation of biofilm architecture, were analyzed by crystal violet (CV) and congo red (CR)-binding assays, respectively. Our data revealed polymicrobial biofilm was more impervious and difficult to eradicate than monomicrobial biofilm[58] (Fig. 6). This may be due to the presence of more than one type of EPS formed by the bacteria which resulted into more viscous matrix[59].

We next perform confocal and scanning electron microscopy to further examine the morphological changes in bacteria after TBO–chit–Au–AgNPs mediated photodynamic therapy, and to elucidate the underlying antibacterial mechanisms. CLSM micrographs illustrate disruption of polymicrobial biofilms of *S. aureus* and *P. aeruginosa* in TBO–chit–Au–AgNPs mediated photodynamic therapy treated group as compared to control and exclusively TBO–chit–Au–AgNPs treated groups. Moreover, the monomicrobial biofilms of *S. aureus* and *P. aeruginosa* was found to be more severely disrupted, almost all the bacterial cells in the biofilms were found dead in TBO–chit–Au–AgNPs mediated PDT group, as compared to control and exclusively TBO–chit–Au–AgNPs treated group (Fig. 7). Thereby, demonstrating strong antibiofilm action of TBO–chit–Au–AgNPs mediated photodynamic therapy (Supplementary Fig. S2). This observation was further supported by the scanning electron microscopy. The control groups of monomicrobial as well as polymicrobial *S. aureus* and *P. aeruginosa* biofilms displayed highly dense and compact microbial cells. While, after treatment with TBO–chit–Au–AgNPs followed by exposure to 100 J/cm$^2$ of laser light, the density of the microbial cells in the monomicrobial as well as in the polymicrobial biofilms of both the species decreases significantly (Fig. 8). Furthermore, TBO–chit–Au–AgNPs mediated photodynamic therapy treated groups showed detrimental effects on cell wall with significant dispersion of the cells leading to leakage of the cellular content, thus obliterating the structural integrity of the biofilm. It has already been reported that Au–Ag nano-shells increases membrane permeability which in turns facilitate the intracellular transport of more AuAg nano-shells, primarily at elevated temperature upon laser irradiation which maximizes the antibacterial efficacy of AuAgNSs[19].

Additionally, the efficacy of TBO–chit–Au–AgNPs mediated photodynamic therapy in healing of diabetic foot ulcer in male wistar rats was checked. Our result showed that daily topical exposure of TBO–chit–Au–AgNPs followed by light irradiation led to marked reduction of *S. aureus* and *P. aeruginosa* colonization in diabetic foot ulcer rats (Fig. 9). Previous study have shown that foot ulcers in the diabetic rats healed slower than those of the non-diabetic rats, however in the present study, TBO–chit–Au–AgNPs mediated PDT remarkably healed foot ulcer in diabetic rats within 7 days, after daily treatment (Fig. 10A–C). Such fast recovery might obviate the chances of having further bacterial infection and consequent mortality. Furthermore, the result of histopathological investigation of monomicrobial and polymicrobial DFU revealed that TBO–chit–Au–AgNPs mediated PDT promotes healing and reduces inflammation in DFU rats (Fig. 11A, B).

Foot ulcers in diabetic patients take a long time to heal due to a series of cellular and molecular mechanism employed in the process of healing, such as neuropathy, high probability of infection, non-physiological inflammatory response, lack of neoangiogenesis, oxidative stress, insufficient concentrations of growth factors, cellular abnormalities, etc.[1,60]. Therefore, in order to understand the pathogenesis and healing of DFU in monomicrobial and polymicrobial state of infection, we have performed serum analysis of several

growth factors and pro-inflammatory cytokines. Our data showed decreased levels of IL-6 and TNF-α in TBO–chit–Au–AgNPs mediated photodynamic therapy treated groups as compared to control, untreated and only TBO–chit–Au–AgNPs treated groups, implying restoration of immunosuppression (Fig. 12-a, b). Furthermore, we have found higher levels of EGF and VEGF in all those groups of rats whose ulcers healed as compared to those groups whose ulcers did not healed (Fig. 12-c, d). This might be, because EGF promote ulcer healing by stimulating cell growth, proliferation and differentiation whereas, VEGF stimulates vasculogenesis and angiogenesis[61,62]. Besides this, elevated level of TGF-β-1 was found in all diabetic groups (with and without foot ulcer) (Fig. 12e). This is because TGF-β-1 is a systemic marker of type-2 diabetes and is positively associated with hyperglycemia. In addition, IGF-1 level was found to be lower in diabetic rats as compared to non-diabetic and control rats. However, considerable decrease was found in DFU rats with polymicrobial infections (Fig. 12f). IGF-1 contributes in cell granulation during wound healing; its expression decreases in diabetic patients which resulted into anomalies in cell granulation[63]. Thus, the findings of present study clearly indicate pathogenesis, healing of DFU and infection control.

## Materials and methods

**Compliance of ethical standards.** This study was carried out in accordance with Institutional Animal Ethics Committee (IAEC) guidelines. The experiments on animals were approved by the "Jawaharlal Nehru Medical College, AMU, Institutional Animal Ethics Committee", registration no. 401/GO/Re/S/2001/CPCSEA. All pertinent guidelines for the care and use of animals have taken in consideration. Moreover, the study reported is in accordance with ARRIVE guidelines.

**Materials.** Chitosan, hydrogen tetrachloroaurate (III) trihydrate ($HAuCl_4{\cdot}3H_2O$) and toluidine blue O (TBO) were procured from Sigma-Aldrich. Ascorbic acid, glacial acetic acid (99.8%), silver nitrate ($AgNO_3$) and sodium hydroxide (NaOH) were purchased from Merck. All reagents used, were of analytical grade and the solutions were prepared using HPLC water. Prior to use, the glacial acetic acid was diluted to a 1% aqueous solution. Chitosan was dissolved in 1% acetic acid solution.

**Nanoparticles synthesis.** Chitosan–coated gold–silver core–shell nanocomposites (chit–Au–AgNPs) were synthesized as described previously. At first, chitosan coated gold nanoparticles termed as 'core' was synthesized by mixing 15 mL of $10 \times 10^{-3}$ M (10 mM) $HAuCl_4$ and 90 mL chitosan solution under magnetic stirring at 50 °C. The appearance of a red color indicates the formation of spherical gold nanoparticles[64].The next step involves 3 consecutive additions of 140 µL of $10 \times 10^{-1}$ M of $AgNO_3$ to a solution containing 70 mL of chit-AuNPs and 560 µL of $10 \times 10^{-1}$ M of ascorbic acid, the latter used as reducing agent in this mixture. After each addition, the mixture was stirred at room temperature for 1 h. Thereafter, $AgNO_3$ was added in a stepwise manner in an attempt to prevent the formation of free Ag nuclei[65].

**Characterization.** The stock solution of TBO was prepared in high performance liquid chromatography (HPLC) grade water. Later, the TBO solution was filtered-sterilized and stored at 4 °C in the dark until used. Further to confirm the conjugation of the TBO to chit–Au–AgNPs, a double-beam UV–visible spectrophotometer (PerkinElmer, Boston, MA, USA) was used. The baseline was fixed in the wavelength range 300–800 nm. We have added TBO (1 mg/mL) serially in 0.5 mM chit–Au–AgNPs and check the UV spectra for their interaction. Transmission electron microscope (TEM, JEM-2100F; Jeol, Tokyo, Japan) was employed to observe the size and morphology of the nanocomposites. The elemental constitution of the synthesized nanocomposites was analyzed using EDS spectroscopic techniques on INCAX-act, Model 51-ADD0076, Oxford instruments. Scanning electron microscopy (SEM) with energy dispersive X-ray spectrometry (EDS) were carried out to verify the presence of gold and silver. Hydrodynamic size and zeta potential of chit-AuNPs, chit–Au–AgNPs and TBO–chit–Au–AgNPs were recorded using Malvern Zetasizer (Nano ZS, Malvern, UK).

**Bacterial strains and culture condition.** *S. aureus* and *P. aeruginosa* were used in this study. Brain heart infusion (BHI) broth (Himedia Labs, Mumbai, India) was used to culture bacteria at 37 °C for 24 h.

**Photosensitization and light source.** Red diode laser (Model No-MRL-III-630; CNI, China) was used for photosensitization.

The effective radiant exposure of the light source was calculated using the following formula[66]:

$$\text{Energy fluency} = \text{Power density} \times \text{Time}$$

where power density (PD) = P (mW)/Area ($cm^2$), P represent the output power (100 mW) of laser and A indicates the area of irradiation. In this study, the laser treatment was carried out in a U-bottom microtiter plate. Thus, the samples acquire the shape of a hemisphere; hence the irradiated area was $2\pi r^2$, where r is the radius of the laser beam exposed, which is equal to 0.35 cm. The beam height from the base was 24.8 mm. Thus, the value of applied PD was 0.1300 W/$cm^2$ and the energy fluency was set to 100 J/$cm^2$ (12 min and 50 s) based on above mentioned formula.

**Estimation of in vitro antibacterial activity by colony forming assay.** *Monomicrobial biofilm. Staphylococcus aureus* and *Pseudomonas aeruginosa* were grown overnight in BHI broth supplemented with 1% sucrose. Thereafter, the cell densities of the suspensions were adjusted to approximately $10^8$ CFU/mL using spectrophotometer (Optical Density; OD 0.8 at 600 nm). Hundred microliters of the diluted bacterial

suspension were added into 96 well plates and incubated for 24 h at 37 °C. After incubation, the biofilms were gently washed with sterile phosphate-buffered saline (PBS) for two times. Subsequently, the preformed biofilm was incubated with TBO–chit–Au–AgNPs in the dark for 30 min and then irradiated with 100 J/cm$^2$ (12 min and 50 s). Control (matured biofilm in phosphate buffer saline) and only TBO–chit–Au–AgNPs treated wells were not exposed to laser light. Finally, the resulting biofilm was then disrupted by vortexing followed by 10-fold serial dilution. 100 µL of the diluted suspension was spread onto BHI agar plate and then incubated at 37 °C for 24 h. A number of grown colonies were imaged and counted[67].

*Polymicrobial biofilms.* To enumerate the CFUs in polymicrobial biofilms, *S. aureus* and *P. aeruginosa* were incubated overnight separately in BHI broth supplemented with 1% sucrose. Polymicrobial or mixed culture biofilms were formed by mixing $10^8$ CFU/mL cells from each bacterial suspension in fresh BHI broth and incubating for 24 h at 37 °C. After incubation, $10^8$ CFU/mL of mixed culture was taken and treated the way as defined above.

*Total ROS detection inside the cells.* 2′,7′-Dichlorofluorescein-diacetate (DCFH-DA) was used to quantify endogenous ROS production in biofilms. Monomicrobial and polymicrobial *S. aureus* and *P. aeruginosa* biofilms were grown for 24 h as described above. After incubation, the cultures were centrifuged at 10,000 × *g* for 15min. Pellets were washed two times with PBS and finally re-suspended in it by adjusting the cell density to $10^8$ CFU/mL followed by incubation for 10 min with 10 µM DCFH-DA. At the end of incubation, the cells were treated with TBO–chit–Au–AgNPs and then irradiated with or without laser light. In, only light treated group, cells were exposed to 100 J/cm$^2$ of laser light. Thereafter, the fluorescence intensity produced from DCFH-DA was estimated by excitation at 485 nm using slit width 1.5 nm[35].

*Evaluation of singlet oxygen in biofilms.* 9, 10-Anthracenediylbis (methylene) dimalonic acid (AMDA) was employed to quantify the $^1O_2$ quantum yields of TBO–chit–Au–AgNPs with and without laser light treatment.

10 µM AMDA was added to the solutions containing monomicrobial and polymicrobial *S. aureus* and *P. aeruginosa* ($10^8$ CFU/mL) biofilms in PBS followed by the treatment as explained above. The reduction in the 399-nm absorption peak of AMDA after treatment corresponds to the amount of singlet oxygen produced[68].O.D in untreated group (control) was taken as 100%.

$$\text{Singlet oxygen generation} = \text{OD of untreated group (control)} - \text{OD of treated group}$$

*Quantification of biofilm formation by crystal violet assay.* Crystal violet assay was performed to quantify the biomass of the monomicrobial and polymicrobial biofilms after treatment with TBO–chit–Au–AgNPs mediated photodynamic therapy. Preformed monomicrobial and polymicrobial biofilms of *S. aureus* and *P. aeruginosa* were grown for 24 h as described in colony forming assay. Prior to the treatment, the exhausted media was removed from each well. Thereafter, the biofilm was incubated with TBO–chit–Au–AgNPs for 30 min and then exposed to laser light (100 J/cm$^2$). Subsequently, the control and treated (only TBO–chit–Au–AgNPs, TBO–chit–Au–AgNPs+ laser light treated) wells of microtiter plates were fixed with formalin (37%, diluted 1:10) and 2% sodium acetate. Biofilms in different groups were stained with 200 µL of crystal violet (0.1%, 15 min). These biofilms were washed twice with PBS; the unbound dye was removed with 100 µL of 95% ethanol. Thereafter, plates were shaken for 10 min to allow full release of the dye and the absorbance was recorded at 630 nm[35].

**Congo red (CR)-binding assay.** The Congo red (CR)-binding assay was conducted to estimate the production of exopolysaccharide (EPS), as reported earlier[69]. Same treatment was given on the preformed biofilm as described above. Thereafter, the exhausted media was removed and wells were washed with PBS twice. Hundred microliters of fresh medium and 50 µL of CR (0.5 mM) were added into each well containing control and treated samples. The mixture solution of fresh medium (100 µL) and CR (50 µL) was also used for blank measurements (blank CR). Subsequently, the microtiter plate was incubated for 2 h at 37 °C. After incubation, the content of each well was transferred to micro-centrifuge tubes followed by centrifugation at 10,000 × g for 5 min. The supernatants were collected and color change was measured at 490 nm[42]. The amount of EPS formed was measured using the following formula[70]:

$$\text{OD of bound CR (EPS produced)} = \text{OD of blank CR} - \text{OD of the supernatant.}$$

**Live/dead staining by CLSM.** Confocal laser scanning microscopy (CLSM) was performed to analyze the consequence of nano photodynamic therapy on monomicrobial and polymicrobial biofilm formation by *S. aureus* and *P. aeruginosa*. Biofilm was grown in covered glass bottom confocal dishes for 24 h at 37 °C. After incubation, unattached bacteria were gently washed away with sterile PBS. The adhered cells or the preformed biofilm was treated as describe above, while controls were left untreated. Then, the biofilm was stained with propidium iodide (PI) and syto9 followed by incubation at 37 °C for 1 h. Thereafter, confocal laser scanning microscope (Fluo View FV1000, TOKYO, JAPAN) was used to image the stained biofilms[35].

**Structural imaging of bacteria in biofilms.** Scanning electron microscopy (SEM) was executed to observe the morphology of *S. aureus* and *P. aeruginosa* monomicrobial as well as polymicrobial biofilms after treatment with TBO–chit–Au–AgNPs followed by exposure to laser light. The preformed biofilm was treated

as describe above. After treatment, biofilms in each sample were fixed with 2% formaldehyde + 2.5% glutaraldehyde in PBS for 2 h at 4 °C. The fixed samples were serially dehydrated with different concentrations of ethanol (20%, 40%, 60%, 80%, and 100%). Finally, the samples were dried, mounted and sputter coated with gold-palladium for SEM analysis[35].

**Cytotoxicity assay.** A cytotoxicity assay was performed on L929 mouse fibroblast cells. The L929 mouse fibroblast cells were grown in Dulbecco's modified Eagles medium (Sigma Aldrich, USA), supplemented with 10% fetal bovine serum (FBS) and 1% antibiotic i.e., penicillin-streptomycin (pen-strep) at 37 °C and 95% humidified incubator with 5% $CO_2$. Sterile conditions were maintained all the times. Cells (~$10^5$cells/well) were seeded in 96-well plates, left overnight to adhere and then treated with various concentrations (0.25 mM, 0.5 mM and 1 mM) of TBO–chit–Au–AgNPs in the presence as well as in the absence of laser irradiation. After 24 h, cell viabilities were determined by methyl thiazolyl tetrazolium (MTT) assay. The medium was removed, and 100 µL of the mixture solution containing fresh medium and MTT (5 mg/mL) solution was added into each well, followed by incubation for 4 h at 37 °C. Subsequently, the formazan crystals formed by the reduction of MTT, were dissolved in DMSO and the absorbance was quantified by measuring its optical density at a wavelength of 570 nm using spectrophotometer[71].

**In vivo study.** A total of 56 adult male wistar rats, weighing, 250–300 g, were used in this study. The rats were equally divided into 6 main groups. Each group and sub-groups consisted of 4 rats each. Group 1 consisted of normal rats without type 2 diabetes mellitus (DM) and foot ulcer (Control); Group 2 contained rats with DM (Untreated); Group 3 consisted of rats with foot ulcer (Untreated); Group 4 contained rats with diabetic foot ulcer (Untreated); Group 5 consisted of diabetic foot ulcer rats treated with TBO–chit–Au–AgNPs while group 6 contained diabetic foot ulcer rats treated with TBO–chit–Au–AgNPs+ laser light (100 J/$cm^2$).

Group 3 to group 6 is further sub-divided into 3 sub-groups, foot ulcerated with monoculture containing *S. aureus*, *P. aeruginosa,* and dual culture (*S. aureus* + *P. aeruginosa*), respectively. The animals were housed 4 per cage and kept on a 12-h light/dark cycle with access to food and water ad libitum.

**Experimental induction of diabetes.** The animals were fasted overnight and diabetes was induced by a single intra-peritoneal injection of a freshly prepared solution of streptozotocin (40 mg/kg b. wt) in 0.1 M citrate buffer (pH 4.5)[1]. Control rats were injected with citrate buffer only. The rats were kept for 14 days to stabilize the diabetic condition.

**Foot ulceration.** Induction of foot ulcer was based on an excisional model. After 14 days treatment of STZ injection, a glucometer was used to determine if each rat's blood glucose level met the severe diabetes level of ≥ 300 mg/dL (hyperglycemia) by drawing blood from the tip of the tail. Rats with a blood glucose level greater than 300 mg/dL were used for foot ulceration. On the day of foot ulceration (Day 0), each rat was anesthetized by intraperitoneal injections of ketamine/xylazine cocktail. The skin surface of the right footpad was shaved and cleaned with 70% ethanol wipe. A 2 mm × 5 mm rectangular full thickness ulcer was created in the skin of the footpad on the right hind leg of each rat using a scalpel[72].

**Treatment of DFU by nano-photodynamic therapy.** The infected foot ulcers were irradiated daily in morning time for 1 week, starting on the 3rd day post infection induction. TBO–chit–Au–AgNPs was added in the middle and spread over the whole infected area. Thirty minutes after the addition, irradiation was carried out with 630 nm of laser light for 12 min and 50 s which corresponds to 100 J/$cm^2$.

**Determination of bacterial load reduction (CFU/mL).** In order to confirm the absence of monomicrobial and polymicrobial *S. aureus* and *P. aeruginosa* colonization, bacterial load was measured for every sample by CFU counting on BHI agar plates and expressed as CFU per mL. Swab samples were collected from the infected foot surfaces of the untreated and treated rats starting on the 3rd, 6th and 9th day post treatment. Collected samples were serially diluted and plated onto BHI agar plates to determine the number of bacteria. The plates were incubated at 37 °C for 24 h before enumeration of colonies.

**Histopathological analysis.** Fresh skin biopsies of control, untreated and treated rat groups were incised and fixed in 10% phosphate buffered formalin (pH 7.4). The tissues were then dehydrated in ascending grades of ethyl alcohol, cleared in xylene and mounted in molten paraplast at 58–62 °C. Thereafter, 5-µm histological sections were cut and stained with haematoxylin and eosin (H/E) to examine microorganism response[73].

**Effects of nano-photodynamic therapy on growth factors and inflammatory cytokines involved in the pathogenesis of diabetic foot ulcers.** To determine the production level of growth factors and inflammatory cytokines, blood samples were drawn under anesthesia and collected into sterile blood collection tubes from the eyes of controls rats, untreated rats, only TBO–chit–Au–AgNPs treated rats and TBO–chit–Au–AgNPs+ laser light treated rats. Thereafter, all rats were immediately sacrificed as per the guidelines. The samples were centrifuged at 5000 rpm for 5 min. Thereafter, the serum supernatant was aliquoted in microcentrifuge tubes and stored at − 80 °C for further analysis[74].The commercially available enzyme-linked immunosorbent assay (ELISA) kits were used according to the manufacturers' protocol: Rat TNF-α (Tumour Necrosis Factor-alpha) ELISA Kit (RAY BIOTECH, CAT: ELR-TNFA), Rat IL-6(Interleukin-6) ELISA Kit (RAY BIOTECH, CAT: ELR-IL6), Rat TGF-β1 (Transforming growth factor beta-1) ELISA Kit (ELABSCIENCE, CAT:

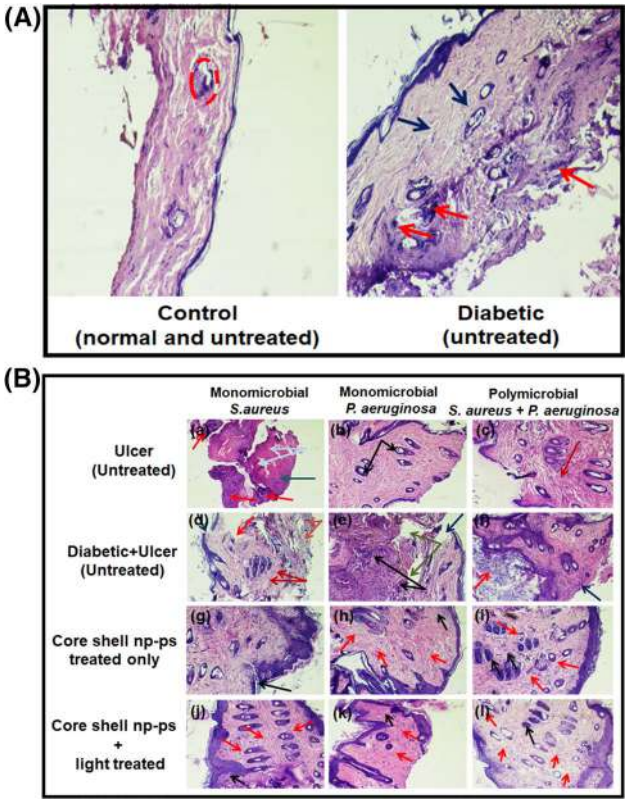


**Figure 11.** Hematoxylin and Eosin (H& E) (×10X) staining to examine response to microorganism of: (**A**) Control and diabetic rats, (**B**) Ulcerated rats (untreated): figure (**a**)–(**c**), DFU rats (untreated): figure (**d**)–(**f**), DFU rats treated with TBO–chit–Au–AgNPs: figure (**g**)–(**i**) and DFU rats treated with TBO–chit–Au–AgNPs + laser: figure (**j**)–(**l**). Red dashed line indicates sebaceous gland in Fig. 10(**A**) Control group, blue arrow indicates thin collagen fibres while red arrow indicates the locations of neutrophils in diabetic group. In Fig. 10(**B**), (a) blue arrow indicates necrosis, grey arrow indicates fibroblasts cells while red arrow indicates dense focal neutrophilic infilterate, (b) black arrow indicates hair follicles, (c) red arrow indicates mild fibrosis, (d) blue arrow indicates ulceration, red arrow indicates collagen fibres, brown arrow indicates thin capillaries while dark brown arrow indicates mild fibrosis, (e) black arrow indicates capillaries, grey arrow indicates collagen fibres while blue arrow indicates ulcer, (f) red arrow indicates squamous epithelium with marked keratosis whereas blue arrow indicates ulcer, (g) black arrow indicates healing ulcer, (h)-(l) red arrow indicates capillaries while black arrow indicates neutrophils.

E-EL-0162), Rat EGF (Epidermal growth factor) ELISA Kit (ELABSCIENCE, CAT: E-EL-R0369), Rat VEGF-A (Vascular endothelial growth factor-A) ELISA Kit (ELABSCIENCE, CAT: E-EL-R2603), Rat IGF-1 (Insulin-like growth factor-1) ELISA Kit (ELABSCIENCE, CAT: E-EL-R3001). The levels of TNF-α, IL-6, TGF-β1, EGF, VEGF-A and IGF-1 were measured by ELISA reader (BIORAD MICROPLATE READER, INDIA).

**Statistical analysis.** All data were presented as averages of the values obtained ± S.D. of three independent experiments. Test groups were compared with the control group using the Student's *t* test and one-way analysis of variance (ANOVA) was used for the comparison of multiple means[75]. For in vivo experiments, all the results were expressed as mean ± S.D. for four rats in each group. Data with $p$ value of less than 0.05 ($^{*}p < 0.01$, $^{**}p < 0.001$, $^{***}p < 0.0001$) was considered statistically significant.

## Conclusion

We have developed a stable and biocompatible chitosan coated gold–silver core–shell nanoparticles conjugated with TBO. The synthesized TBO–chit–Au–AgNPs mediated photodynamic therapy was used for the first time to eliminate multi-drug resistant Gram-positive, and Gram-negative, monomicrobial as well as polymicrobial biofilms. Furthermore, this novel nano-phototheranostic complex proved as a nontoxic antibacterial agent to combat DFU caused by multi-drug resistant bacterial strains. Therefore, this approach holds a promising potential to be validated and implemented in clinical translation.

Received: 1 June 2021; Accepted: 16 November 2021
Published online: 27 December 2021

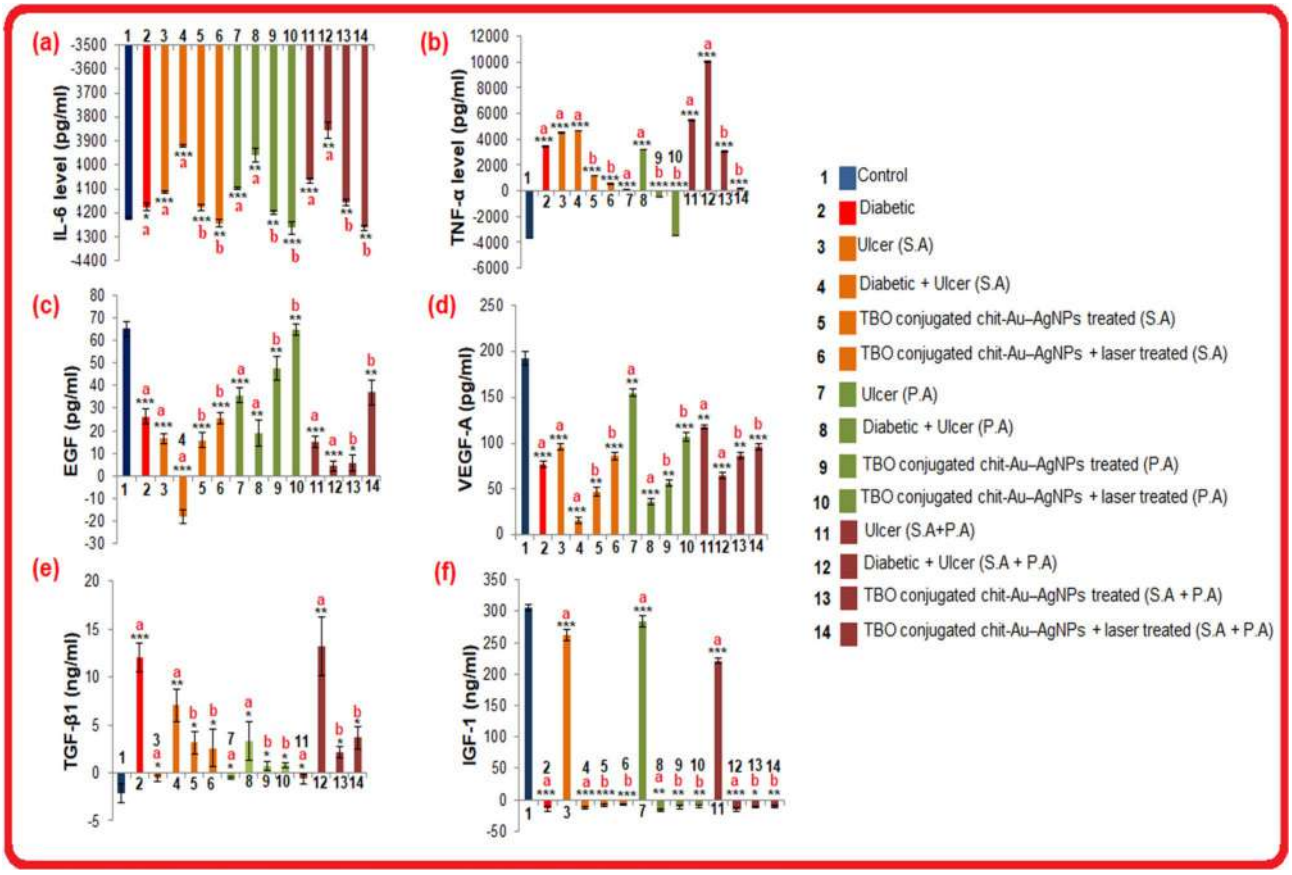


**Figure 12.** Effect of TBO–chit–Au–AgNPs mediated photodynamic therapy on pro-inflammatory cytokines and growth factors levels in Control rats, STZ induced diabetic rats (untreated), Ulcerated rats (untreated), DFU rats (untreated), DFU rats treated with TBO–chit–Au–AgNPs, DFU rats treated with TBO–chit–Au–AgNPs + laser: (**a**) IL-6 level, (**b**) TNF-α level, (**c**) EGF level, (**d**) VEGF-A level, (**e**) TGF-β1 level and (**f**) IGF-1 level. Each bar represents mean ± SD of 4 rats. Significance at: p-value *p < 0.01, **p < 0.001, ***p < 0.000, ns = not significant. a—compared with control or normal rats; b—compared with untreated diabetic foot ulcer rats.

## References


1. Yu, C. O.-L., *et al.* The characterization of a full-thickness excision open foot wound model in n5-streptozotocin (STZ)-induced type 2 diabetic rats that mimics diabetic foot ulcer in terms of reduced blood circulation, higher C-reactive protein, elevated inflammation, and reduced cell proliferation. *Exp. Anim.* **66**(3), 259–269 (2017).
2. Falanga, V. Wound healing and its impairment in the diabetic foot. *The Lancet* **366**(9498), 1736–1743 (2005).
3. Kwon, K. T. & David, G. A. Microbiology and antimicrobial therapy for diabetic foot infections. *Infect. Chemother.* **5**0(1), 11–20 (2018).
4. Blakytny, R., and Jude, E. The molecular biology of chronic wounds and delayed healing in diabetes. *Diabetic Med.* **23**, 594–608 (2006).
5. Lan, C.-C.E., *et al.* Hyperglycaemic conditions decrease cultured keratinocyte mobility: implications for impaired wound healing in patients with diabetes. *Br. J. Dermatol.* **159**, 1103–1115 (2008).
6. Spollett, G. R. Preventing amputations in the diabetic population. *Nurs. Clin. N. Am.* **33**, 629–641 (1998).
7. Dunne Jr, W. M. Bacterial adhesion: Seen any good biofilms lately? *Clin. Microbiol. Rev.* **15**, 155–166 (2002).
8. Petersen, E. International Journal of Infectious Diseases. 16th International Congress on Infectious Diseases (ICID). Cape Town: Elsevier, 2014.
9. Lasa Uzcudun, Í. Towards the identification of the common features of bacterial biofilm development. *Int. Microbiol.* **9**(1), 21–28 (2006).
10. De la Fuente-Núñez, C., *et al.* Broad-spectrum anti-biofilm peptide that targets a cellular stress response. *PLoS Pathog.* **10**, e1004152 (2014).
11. Lipsky, B. A., *et al.* Diagnosis and treatment of diabetic foot infections. *J. Am. Podiatr. Med. Assoc.* **95**, 183–210 (2005).
12. Stacy, A., *et al.* The biogeography of polymicrobial infection. *Nat. Rev. Microbiol.***14**, 93–105 (2016).
13. Ferrer-Espada, R., *et al.* Antimicrobial blue light inactivation of polymicrobial biofilms. *Front. Microb.* **10**, 721 (2019).
14. DeLeon, S., *et al.* Synergistic interactions of *Pseudomonas aeruginosa* and *Staphylococcus aureus* in an in vitro wound model. *Infect. Immun.* **82**, 4718–4728 (2014).
15. Nguyen, A. T. & Oglesby-Sherrouse, A. G. Interactions between *Pseudomonas aeruginosa* and *Staphylococcus aureus* during co-cultivations and polymicrobial infections. *Appl. Microbiol. Biotechnol.* **100**(14), 6141–6148 (2016).
16. Wolcott, R. *et al.* The polymicrobial nature of biofilm infection. *Clin. Microbiol. Infect.* **19**(2), 107–112 (2013).
17. Parveen, S., Misra, R. & Sahoo, S. K. Nanoparticles: a boon to drug delivery, therapeutics, diagnostics and imaging. *Nanomed. Nanotechnol. Biol. Med.* **8**, 147–166 (2012).
18. Gold, K., *et al.* Antimicrobial activity of metal and metal-oxide based nanoparticles. *Adv. Ther.* **1**, 1700033 (2018).
19. He, J., *et al.* Gold–silver nanoshells promote wound healing from drug-resistant bacteria infection and enable monitoring via surface-enhanced Raman scattering imaging. *Biomater.* **234**, 119763 (2020).

20. Khan, A. K. *et al.* Gold nanoparticles: Synthesis and applications in drug delivery. *Trop. J. Pharm. Res.* **13**(7), 1169–1177 (2014).
21. Dhamecha, D., Jalalpure, S. & Jadhav, K. Nepenthes khasiana mediated synthesis of stabilized gold nanoparticles: Characterization and biocompatibility studies. *J. Photochem. Photobiol. B* **154**, 108–117 (2016).
22. Giljohann, D. A., *et al.* Gold nanoparticles for biology and medicine. *Angew. Chem. Int. Edn.* **49**, 3280–3294 (2010).
23. Salem, D. S., *et al.* Improved chemo-photothermal therapy of hepatocellular carcinoma using chitosan–coated gold nanoparticles. *J. Photochem. Photobiol. B* **182**, 92–99 (2018).
24. Hada, A.-M., *et al.* Fabrication of gold–silver core–shell nanoparticles for performing as ultrabright SERS-nanotags inside human ovarian cancer cells. *Nanotechnol.* **30**, 315701 (2019).
25. Sondi, I. & Branka, S.-S. Silver nanoparticles as antimicrobial agent: A case study on *E. coli* as a model for Gram-negative bacteria. *J. Colloid Interface Sci.* **275**, 177–182 (2004).
26. Potara, M., *et al.* Synergistic antibacterial activity of chitosan–silver nanocomposites on *Staphylococcus aureus*. *Nanotechnology* **22**, 135101 (2011).
27. Morones, J. R., *et al.*The bactericidal effect of silver nanoparticles. *Nanotechnol.* **16**, 2346 (2005).
28. Li, Q., *et al.* Antimicrobial nanomaterials for water disinfection and microbial control: potential applications and implications. *Water Res.* **42**, 4591–4602 (2008).
29. Rabea, E. I., *et al.* Chitosan as antimicrobial agent: Applications and mode of action. *Biomacromolecules* **4**, 1457–1465 (2003).
30. Chen, Q., *et al.* Preparation, antibacterial, and antioxidant activities of silver/chitosan composites. *J. Carbohydr. Chem.* **33**, 298–312 (2014).
31. Sharma, M., *et al.* Toluidine blue-mediated photodynamic effects on staphylococcal biofilms. *Antimicrob. Agents Chemother.* **52**, 299–305 (2008).
32. Demidova, T. N. & Hamblin, M. R. Effect of cell-photosensitizer binding and cell density on microbial photoinactivation. *Antimicrob. Agents Chemother.* **49**(6), 2329–2335 (2005).
33. Usacheva, M. N., Teichert, M. C. & Biel, M. A. Comparison of the methylene blue and toluidine blue photobactericidal efficacy against gram-positive and gram-negative microorganisms. *Lasers Surg. Med.* **29**, 165–173 (2001).
34. Wainwright, M. Photodynamic antimicrobial chemotherapy (PACT). *J. Antimicrob. Chemother.* **42**(1), 13–28 (1998).
35. Misba, L., Zaidi, S. & Khan, A. U. A comparison of antibacterial and antibiofilm efficacy of phenothiazinium dyes between Gram positive and Gram negative bacterial biofilm. *Photodiagn. Photodyn. Ther.* **18**, 24–33 (2017).
36. Misba, L., Abdulrahman, H. & Khan, A. U. Photodynamic efficacy of toluidine blue O against mono species and dual species bacterial biofilm. *Photodiagn. Photodyn. Ther.* **26**, 383–388 (2019).
37. Costa, L., *et al.* Involvement of type I and type II mechanisms on the photoinactivation of non-enveloped DNA and RNA bacteriophages. *J. Photochem. Photobiol. B* **120**, 10–16 (2013).
38. Carvalho, C. M. B., *et al.* Photoinactivation of bacteria in wastewater by porphyrins: Bacterial β-galactosidase activity and leucine-uptake as methods to monitor the process. *J. Photochem. Photobiol. B* **88**, 112–118 (2007).
39. Almeida, A., Faustino, M. A. F. & Tomé, J. P. C.. Photodynamic inactivation of bacteria: Finding the effective targets. *Future Med. Chem.* **7**, 1221–1224 (2015).
40. Hamblin, M. R. & Hasan, T. Photodynamic therapy: A new antimicrobial approach to infectious disease?. *Photochem. Photobiol. Sci.* **3**(5), 436–450 (2004).
41. Costa, L., *et al.* Photodynamic inactivation of mammalian viruses and bacteriophages. *Viruses* **4**, 1034–1074 (2012).
42. da Silva, Raquel N., *et al.* Photo-inactivation of Bacillus endospores: Inter-specific variability of inactivation efficiency. *Microbiol. Immunol.* **56**, 692–699 (2012).
43. Maisch, T. *et al.* Determination of the antibacterial efficacy of a new porphyrin-based photosensitizer against MRSA ex vivo. *Photochem. Photobiol. Sci.* **6**(5), 545–551 (2007).
44. Rodrigues, G. B., *et al.* Susceptibilities of the dermatophytes *Trichophyton mentagrophytes* and *T. rubrum microconidia* to photodynamic antimicrobial chemotherapy with novel phenothiazinium photosensitizers and red light. *J. Photochem. Photobiol. B* **116**, 89–94 (2012).
45. Rodrigues, G. B., *et al.* In vitro photodynamic inactivation of Candida species and mouse fibroblasts with phenothiazinium photosensitisers and red light. *Photodiagn. Photodyn. Ther.* **10**, 141–149 (2013).
46. Beirao, S., *et al.* Photodynamic inactivation of bacterial and yeast biofilms with a cationic porphyrin. *Photochem. Photobiol.* **90**, 1387–1396 (2014).
47. Cieplik, F., *et al.* Antimicrobial photodynamic therapy—what we know and what we don't. *Crit. Rev. Microbiol.* **44**, 571–589 (2018).
48. Huang, Y.-Y., *et al.* Antimicrobial photodynamic therapy mediated by methylene blue and potassium iodide to treat urinary tract infection in a female rat model. *Sci. Rep.* **8**, 1–9 (2018).
49. Khan, S., *et al.* Photoinactivation of multidrug resistant bacteria by monomeric methylene blue conjugated gold nanoparticles. *J. Photochem. Photobiol. B* **174**, 150–161 (2017).
50. Akhtar, F., *et al.* Antimicrobial and antibiofilm photodynamic therapy against vancomycin resistant *Staphylococcus aureus* (VRSA) induced infection in vitro and in vivo. *Eur. J. Pharmaceut Biopharmaceut* **160**, 65–76 (2021).
51. Ahmed, D. N., *et al.* Waste foundry sand/MgFe-layered double hydroxides composite material for efficient removal of Congo red dye from aqueous solution. *Sci. Rep.* **10**, 1–12 (2020).
52. Zhang, X., *et al.* Mass production of poly(ethylene glycol) monooleate-modified core–shell structured upconversion nanoparticles for bio-imaging and photodynamic therapy. *Sci. Rep.* **9**, 1–10 (2019).
53. Lu, L., *et al.* Core–shell gold/silver nanoparticles: Synthesis and optical properties. *J. Colloid Interface Sci.* **392**, 90–95 (2013).
54. Kumar, M. N. V. Ravi, *et al.* Chitosan chemistry and pharmaceutical perspectives. *Chem. Rev.* **104**, 6017–6084 (2004).
55. Misba, L. & Khan, A. U. Enhanced photodynamic therapy using light fractionation against *Streptococcus mutans* biofilm: Type I and type II mechanism. *Future Microbiol.* **13**(4), 437–454 (2018).
56. Caudill, Emily R., *et al.* Wall teichoic acids govern cationic gold nanoparticle interaction with Gram-positive bacterial cell walls. *Chem. Sci.* **11**, 4106–4118 (2020).
57. Kim, S. Y., Kwon, O. J. & Park, J.-W. Inactivation of catalase and superoxide dismutase by singlet oxygen derived from photoactivated dye. *Biochimie* **83**, 437–444 (2001).
58. Pereira, C. A., *et al.* Susceptibility of *Candida albicans, Staphylococcus aureus*, and *Streptococcus mutans* biofilms to photodynamic inactivation: an in vitro study. *Lasers Med. Sci.* **26**, 341–348 (2011).
59. Skillman, L. C., Sutherland, I. W. & Jones, M. V. The role of exopolysaccharides in dual species biofilm development. *J. Appl. Microbiol.* **85**(S1), 13S-18S (1998).
60. Vlassara, H., *et al.* Identification of galectin-3 as a high-affinity binding protein for advanced glycation end products (AGE): A new member of the AGE-receptor complex. *Mol. Med.* **1**, 634–646 (1995).
61. Ojalvo, A. G., *et al.* Healing enhancement of diabetic wounds by locally infiltrated epidermal growth factor is associated with systemic oxidative stress reduction. *Int. Wound J.* **14**, 214–225 (2017).
62. Gardner, J. C., *et al.* Keratinocyte growth factor supports pulmonary innate immune defense through maintenance of alveolar antimicrobial protein levels and macrophage function. *Am. J. Physiol. Lung Cell. Mol. Physiol.* **310**, L868–L879 (2016).
63. Zubair, M. & Ahmad, J. Role of growth factors and cytokines in diabetic foot ulcer healing: A detailed review. *Rev. Endocr. Metab. Disord.* **20**(2), 207–217 (2019).

64. Aldea, M., *et al.* Metformin delivery using chitosan–capped gold nanoparticles in glioblastoma cell lines. *Roman. Neurosurg.* 230–239 (2018).
65. Samal, A. K., *et al.* Size tunable Au@ Ag core–shell nanoparticles: Synthesis and surface-enhanced Raman scattering properties. *Langmuir* **29**, 15076–15082 (2013).
66. Rolim, J. P. M. L., *et al.* The antimicrobial activity of photodynamic therapy against *Streptococcus mutans* using different photosensitizers. *J. Photochem. Photobiol. B* **106**, 40–46 (2012).
67. Misba, L., Kulshrestha, S. & Khan, A. U. Antibiofilm action of a toluidine blue O-silver nanoparticle conjugate on *Streptococcus mutans*: A mechanism of type I photodynamic therapy. *Biofouling* **32**, 313–328 (2016).
68. Chen, J., Cesario, T. C. & Rentzepis, P. M. Rationale and mechanism for the low photoinactivation rate of bacteria in plasma. *Proc. Natl. Acad. Sci.* **111**(1), 33–38 (2014).
69. Kulshrestha, S., *et al.* Calcium fluoride nanoparticles induced suppression of *Streptococcus mutans* biofilm: An in vitro and in vivo approach. *Appl. Microbiol. Biotechnol.* **100**, 1901–1914 (2016).
70. López-Moreno, A., *et al.* Calcium carbonate precipitation by heterotrophic bacteria isolated from biofilms formed on deteriorated ignimbrite stones: Influence of calcium on EPS production and biofilm formation by these isolates. *Biofouling* **30**, 547–560 (2014).
71. Senapati, .V A., *et al.* ZnO nanoparticles induced inflammatory response and genotoxicity in human blood cells: A mechanistic approach. *Food Chem. Toxicol.* **85**, 61–70 (2015).
72. Lau, T. W. *et al.* An in vivo investigation on the wound-healing effect of two medicinal herbs using an animal model with foot ulcer. *Eur. Surg. Res.* **41**(1), 15–23 (2008).
73. Tawfik, A. A. *et al.* A study of the treatment of cutaneous fungal infection in animal model using photoactivated composite of methylene blue and gold nanoparticle. *Photodiagn. Photodyn. Ther.* **15**, 59–69 (2016).
74. Karamese, M., *et al.* Anti-oxidant and anti-inflammatory effects of apigenin in a rat model of sepsis: an immunological, biochemical, and histopathological study. *Immunopharmacol. Immunotoxicol.* **38.3**, 228–237 (2016).
75. ANOVA: Analysis OfVAriance between groups. www.physics.csbsju.edu/stats/anova.html


## Acknowledgements

The authors would like to acknowledge university sophisticated instruments facility (USIF), AMU, for providing instrumental support. This work was financially supported by Department of Science and Technology Research Grant, DST: SR/NM/NS-41/2016(G). FA acknowledged fellowship from Council of Scientific and industrial research: 09/112(0600)/2018-EMR-I.

## Author contributions

F.A., performed all experiments and wrote manuscript, A.U.K., designed problem, guided whole study and check draft manuscript, B.Q., help in animal study, S.G., help and perform cell line experiments to check cytotoxicity, P.M., provide cell culture facility and help interpreting toxicity data, K.A., is pathologist, performed all pathology analysis and A.A. has provided animal facility.

## Funding

Science and Engineering Research Board (Grant No. SR/NM/NS-41/2016(G)).

## Competing interests

The authors declare no competing interests.

## Additional information

**Supplementary Information** The online version contains supplementary material available at https://doi.org/10.1038/s41598-021-04008-x.

**Correspondence** and requests for materials should be addressed to A.U.K.

**Reprints and permissions information** is available at www.nature.com/reprints.

**Publisher's note** Springer Nature remains neutral with regard to jurisdictional claims in published maps and institutional affiliations.

European Journal of Pharmaceutics and Biopharmaceutics 160 (2021) 65–76

Contents lists available at ScienceDirect

European Journal of Pharmaceutics and Biopharmaceutics

journal homepage: www.elsevier.com/locate/ejpb

# Antimicrobial and antibiofilm photodynamic therapy against vancomycin resistant *Staphylococcus aureus* (VRSA) induced infection in vitro and in vivo

Farheen Akhtar [a], Asad U. Khan [a,*], Lama Misba [a], Kafil Akhtar [b], Asif Ali [c]

[a] Medical Microbiology and Molecular Biology Lab., Interdisciplinary Biotechnology Unit, Aligarh Muslim University, Aligarh, India
[b] Department of Pathology, JNMC, A.M.U., Aligarh, India
[c] Department of Biochemistry, F/o Medicine, JNMC A.M.U., Aligarh, India

ARTICLE INFO

*Keywords:*
Antimicrobial photodynamic therapy (aPDT)
Antimicrobial resistance
Preformed-biofilm
Curcumin
Blue laser light
Vancomycin resistant *Staphylococcus aureus* (VRSA)
Skin abrasion
Rat model
Cytokine profiling

ABSTRACT

Biofilm mediated infection caused by multi-drug resistant bacteria are difficult to treat since it protects the microorganisms by host defense system, making them resistant to antibiotics and other antimicrobial agents. Combating such type of nosocomial infection, especially in immunocompromised patients, is an urgent need and foremost challenge faced by clinicians. Therefore, antimicrobial photodynamic therapy (aPDT) has been intensely pursued as an alternative therapy for bacterial infections. aPDT leads to the generation of reactive oxygen species (ROS) that destroy bacterial cells in the presence of a photosensitizer, visible light and oxygen. Here, we elucidated a possibility of its clinical application by reducing the treatment time and exposing curcumin to 20 J/cm$^2$ of blue laser light, which corresponds to only 52 s to counteract vancomycin resistant *Staphylococcus aureus* (VRSA) both in vitro and in vivo. To understand the mechanism of action, the generation of total reactive oxygen species (ROS) was quantified by 2′-7′-dichlorofluorescein diacetate (DCFH-DA) and the type of phototoxicity was confirmed by fluorescence spectroscopic analysis. The data showed more production of singlet oxygen, indicating type-II phototoxicity. Different anti-biofilm assays (crystal violet and congo red assays) and microscopic studies were performed at sub-MIC concentration of curcumin followed by treatment with laser light against preformed biofilm of VRSA. The result showed significant reduction in the preformed biofilm formation. Finally, its therapeutic potential was validated in skin abrasion wistar rat model. The result showed significant inhibition of bacterial growth. Furthermore, immunomodulatory analysis with rat serum was performed. A significant reduction in expression of proinflammatory cytokines TNF-α and IL-6 were observed. Hence, we conclude that curcumin mediated aPDT with 20 J/cm$^2$ of blue laser treatment (for 52 s) could be used against multi-drug resistant bacterial infections and preformed biofilm formation as a potential therapeutic approach.

## 1. Introduction

The multidrug-resistant (MDR) bacterial infections have been considered as a global threat [1]. Colistin, a class of polypeptide, which is being used as 'last-line' of defense against MDR infections, has also been proved to be ineffective due to resistance emergence [2]. Due to this therapeutic failure, new strategies need to be developed to combat with these emerging infections [3]. Such infections are even tough to treat in case of biofilm formation, being protected by host defense system, which make them less susceptible to antimicrobial. In recent decades, the treatment of *Staphylococcus aureus* biofilm mediated infections has become more difficult as the prevalence of multi-drug resistant continues to upsurge. These foremost challenges have motivated many researchers in the prevailing situation to develop alternative therapeutic options. Consequently, antimicrobial photodynamic therapy (aPDT) has been emerged as a promising alternative approach against bacterial infections [4]. It has been used successfully for curing several diseases like cancer [5], age related macular degeneration [6,7], rheumatoid arthritis [8], skin disease [9–11] and arteriosclerosis [12]. Apart from this, various studies have been published depicting the effectiveness of photodynamic therapy against Gram-negative bacteria, Gram-positive bacteria, viruses, fungi, and parasites [11,13–22]. The

* Corresponding author at: Medical Microbiology and Molecular Biology Lab., Interdisciplinary Biotechnology Unit, Aligarh Muslim University, Aligarh 202002, UP, India.
*E-mail address:* asadukhan72@gmail.com (A.U. Khan).

https://doi.org/10.1016/j.ejpb.2021.01.012
Received 10 July 2020; Received in revised form 22 December 2020; Accepted 20 January 2021
Available online 25 January 2021

concept of antimicrobial photodynamic therapy is quite upfront and holds a promising modality in the treatment of microorganisms. It is based on a simple concept of using light of visible wavelength range, causing rapid and complete killing of microorganisms by generating highly reactive oxygen species (ROS) after their sensitization with a nontoxic photoactive drug in the presence of oxygen [23].

A photoactive drug or a photosensitizer should have a strong absorption peak in range of 650 nm to 800 nm (red to near-infrared), spectral region. Moreover, an ideal photosensitizer should possess a significant triplet quantum yield leading to ample production of ROS upon irradiation by controlled light sources, such as lasers and light emitting diode (LED) [24–26].

The mechanism of action involved in antimicrobial photodynamic therapy is merely dependent upon the ability of a photosensitizer to generate ROS on light irradiation. The non-toxic photosensitizer absorbs photons of light of the appropriate wavelength to get excited. Once excited, photosensitizer gets converted from excited singlet state to a long lived excited triplet state through intersystem crossing which subsequently reacts with ground (triplet) state $O_2$ in two different ways [27]. In type-I reaction, it transfer electron to substrate (eg. lipid, nucleic acid and proteins) which leads to the formation of free radicals like hydroxyl radicals ($OH^{\bullet}$), hydrogen peroxide ($H_2O_2$) and superoxide ($O^{2-}$). Whereas, in type-II reaction it involves transfer of energy to molecular oxygen which leads to the generation of singlet state oxygen [28]. Due to non-specific nature of the death caused by ROS, and shorter exposure time to the photosensitizer, the expression of protective factors involved in the development of resistance is slowed down, making it difficult for bacterial cells to acquire resistance against antimicrobial photodynamic therapy [3].

Among different types of photosensitizers (chlorothiazides, porphyrins, phenothiazines, sulfonamides, and tetracyclines) known, Curcumin is one of the commonly used natural photosensitizer [29–32]. It is a polyphenolic compound from the spice turmeric (*Curcuma longa L.*) and has been identified as an efficient photosensitizer for inactivation of a broad range of microorganisms. It shows antimicrobial, antioxidant, anti-inflammatory, antitumor and antifungal properties [33–38]. Furthermore, curcumin plays a significant role in the process of wound healing by down regulating the production of pro-inflammatory cytokines such as tumor necrosis factor-alpha (TNFα) and interleukins (ILs); stimulating healing growth factors, increasing fibroblast numbers, antioxidant enzymes, granulation tissue formation, and collagen deposition; and accelerating neovascularization, re-epithelialization and wound closure [39–43]. The therapeutic potential of curcumin is further enhanced because of its ability to absorb blue light in the wavelength range 400–500 nm of the visible spectrum [44].Therefore, in view of above background, we have initiated to investigate the efficacy of curcumin mediated antimicrobial photodynamic therapy, to inhibit multidrug resistant infection in vitro as well as in vivo using VRSA induced skin abrasion both in normal and immunocompromised wistar rats that have been rendered temporarily neutropenic by cyclophosphamide administration.

## 2. Materials and methods

### 2.1. Compliance with ethical standards

This research was conducted in accordance with institutional ethical standards. The study on animals was approved by the "Jawaharlal Nehru Medical College, AMU, Institutional Animal Ethics Committee", registration no. 401/GO/Re/S/2001/CPCSEA. All applicable international, national, and/or institutional guidelines for the care and use of animals were followed.

### 2.2. Bacterial strain and isolate identification

Clinical sample was collected from the burn patient with a sterile swab and cultured on brain heart infusion (BHI) broth (HIMEDIA LABS, MUMBAI, INDIA) for 24 h and incubated at 37 °C [45].

BD Phoenix$^{TM-100}$ automated microbiology system (Gram positive susceptibility card) was used for primary identification. The species level identification of isolate was performed by 16 s rDNA sequencing. The strain was identified as *Staphylococcus aureus*. The pure culture of isolate was cryopreserved at −80 °C in 70% glycerol.

### 2.3. Antimicrobial susceptibility testing

Antimicrobial susceptibility was determined by the standard disc diffusion method using Mueller Hinton (MH) agar plates (HIMEDIA LABS, MUMBAI, INDIA) as per the Clinical and Laboratory Standards Institute (CLSI, 2016) guidelines. These antibiotics discs (vancomycin, colistin, polymyxin, ceftazidime, amikacin, aztreonam) were used in this study. This test was performed only to determine the antibiotic susceptibility of the isolated strain that will be further used with curcumin

### 2.4. Determination of bacteriostatic (MIC) and bactericidal (MBC) concentrations

Curcumin (HIMEDIA LABS, MUMBAI, INDIA) was used as photosensitizer. The stock solution of curcumin (20 mg/ml) was prepared in DMSO and stored at 4 °C in the dark. The minimum inhibitory concentration (MIC) of curcumin against VRSA was determined by microdilution method as per Clinical and Laboratory Standards Institute (CLSI) guidelines [46]. Stock solution of curcumin was serially diluted with BHI media in 96 well microtiter plate. Bacterial cell density was estimated by spectrophotometry (Optical Density; OD 0.8 at 600 nm). Diluted overnight culture ($10^8$ CFU/ml) was added in each well followed by irradiation of 20 J/cm$^2$ with 405 nm wavelength blue laser light. The treated cells were incubated for 24 h at 37 °C. MICs were determined as the lowest concentration that completely inhibits visible bacterial growth whereas, MBC were determined by sub-culturing the test dilution on MH agar plates.

### 2.5. Photosensitization and light source

Diode laser (Model No-MDL-III-405; CNI, China) was used for photosensitization.

The effective radiant exposure of the light source was calculated as follows [47]:

Energy fluency = Power density × Time

Where, power density (PD) is PD = P (mW)/Area (cm$^2$), P is the output power of the light source (300 mW) and A is the irradiated area. In the present study the photodynamic treatment was carried out in a U-bottom microtiter plate. Therefore, samples acquire the shape of a hemisphere; hence the irradiated area was $2\pi r^2$, where r is the radius of the laser beam exposed, equal to 0.35 cm. The beam height from the base was 24.8 mm. The applied PD was 389.96 mW/cm$^2$ and the energy fluency was set to 20 J cm$^{-2}$ when irradiated for 52 s.

### 2.6. Detection of total ROS inside the cells

Endogenous ROS production after aPDT was quantified by fluorescence spectroscopy using 2′, 7′- dichlorofluorescein-diacetate (DCFH-DA, SIGMA-ALDRICH, USA, CAS NUMBER: 4091-99-0). Overnight culture was centrifuged at 10,000*g* for 15 min. Pellets were washed twice with phosphate buffer saline at pH 7.4 and finally re-suspended in PBS by adjusting the cell density to $10^8$ CFU/ml followed by incubation for 10 min with 10 μM DCFH-DA. At the end of incubation, the cells were treated with sub-MIC concentration (78 μg/ml) of curcumin and irradiated with 20 J/cm$^2$ of light dose corresponding to 52 s while the control (PBS) was left untreated. In only light treated group, we have irradiated cells with 20 J/cm$^2$ laser light without curcumin. Thereafter, the fluorescence intensity produced from DCFH-DA was measured by

excitation at 485 nm using slit width 1.5 nm [48].

### 2.7. Fluorescence probe experiments

Fluorescence probe (hydroxyphenyl fluorescein [HPF]) was used to determine the $HO^{\bullet}$ produced by curcumin upon irradiation [49]. The bacterial suspension ($10^8$ CFU/ml) was incubated with HPF (final concentration of 10 μM) for 10 min in PBS. After incubation, the cells were treated with sub-MIC concentration of curcumin and irradiated with 20 J/cm$^2$ of light dose corresponding to 52 s in aPDT treated group while the control was left untreated. The fluorescence intensity was measured by excitation at 492 nm using slit width 1.5 nm [48].

### 2.8. Detection of singlet oxygen

9, 10-Anthracenediylbis (methylene) dimalonic acid (AMDA, SIGMA-ALDRICH, USA, CAS NUMBER: 307554-62-7) was used to quantify the $^1O_2$ quantum yields of curcumin. 10 μM AMDA was added to solution containing VRSA ($10^8$ CFU/ml) in PBS followed by the treatment as explained above. The relative amount of $^1O_2$ generated in each solution was determined by recording the decrease in the 399-nm absorption band of AMDA as a function of 405 nm of laser light irradiation. The 399-nm OD (optical density) decay is a measure of the amount of $^1O_2$ generated [50].

### 2.9. In vitro estimation of VRSA load reduction by colony forming unit (CFU/ml)

The efficacy of curcumin mediated aPDT on the viability of vancomycin resistant *Staphylococcus aureus* preformed biofilm was investigated using following protocol. Overnight culture of VRSA was re-suspended to a final concentration of $10^8$ CFU/mL in fresh BHI supplemented with 1% sucrose. Aliquots (100 μl) of the diluted bacterial suspension were added in each well of 96 well microtitre plate and incubated for 24 h at 37 °C. Prior to the treatment, the remaining non-adherent bacteria were removed by washing with sterile PBS. Thereafter, preformed biofilm was incubated with sub-MIC concentration of curcumin in the dark for 30 min and then treated with 20 J/cm$^2$ energy density blue laser light. Control (matured biofilm in phosphate buffer saline without any treatment) was left untreated. Biofilm was then disrupted by vortexing followed by 10 fold serial dilution. 100 μl aliquots were plated onto BHI agar plate and incubated at 37 °C for 24 h. A number of grown colonies were then counted [51].

### 2.10. Quantification of biofilm formation by crystal violet assay

Biofilm formation by VRSA, after treatment with curcumin-aPDT (curcumin-antimicrobial photodynamic therapy), was evaluated using crystal violet assay. Preformed biofilm was grown for 24 h as described in bacterial load reduction (CFU/ml). Prior to the treatment, the exhausted media was removed from each well. Thereafter, the biofilm was incubated with sub-MIC concentration of curcumin for 30 mins followed by 20 J/cm$^2$ of irradiation, corresponding to 52 s in aPDT treated group. Control was left untreated. Subsequently, the control and treated biofilm-coated wells of microtiter plates were fixed with formalin (37%, diluted 1:10) and 2% sodium acetate. Biofilms in all the wells were subsequently stained using 200 μl of 0.1% crystal violet for 15 min at room temperature. After two rinses with sterile PBS, unbound dye was removed from the cells with 100 μl of 95% ethanol. The plates were shaken for 10 min to allow full release of the dye and the absorbance was recorded by measuring optical density of suspension at 630 nm by microplate reader (BIORAD MICROPLATE READER, INDIA) [48]. The amount of EPS produced was estimated using the following formula described by López-Moreno *et al.*, 2014 [52].

OD of blank CR-OD of the supernatant = OD of bound CR (EPS produced)

### 2.11. Estimation of exopolysaccharide production

The Congo red (CR)-binding assay was used to estimate the production of exopolysaccharide (EPS), as reported earlier [53]. Same photodynamic treatment was given on preformed biofilm as described above. After treatment exhausted media were removed and wells were washed twice with PBS. 100 μl of fresh media and 50 μl of CR (0.5 mM) were then added to each wells containing control and treated samples. 100 μl of medium along with 50 μl CR was also used for blank measurements (blank CR). Thereafter, the microtiter plate was incubated for 2 h at 37 °C. After incubation, the contents of each wells was transferred to micro-centrifuge tubes followed by centrifugation at 10,000*g* for 5 min. The supernatants were transferred to fresh microtiter plate and colorimetric change was measured using microtiter plate reader (BIO-RAD iMark TM Microplate reader) at 490 nm [18].

### 2.12. Confocal laser scanning microscopy (CLSM)

Confocal laser scanning microscopy (CLSM) was performed to analyze the consequence of curcumin mediated antimicrobial photodynamic therapy on VRSA biofilm after irradiation with 20 J/cm$^2$ of light dose. Biofilm was grown in covered glass bottom confocal dishes (GENETIX BIOTECH ASIA PVT. LTD., NEW DELHI, INDIA) for 24 h at 37 °C. After incubation, sterile PBS was used to wash the confocal dishes to remove the loosely bound cells. The adhered cells or the preformed biofilm was treated as describe above, while controls were left untreated. Thereafter, the biofilm was then stained with propidium iodide (PI) and syto9 followed by incubation at 37 °C for 1 h. Fluorescence emission was observed using Fluo View FV1000 (OLYMPUS, TOKYO, JAPAN) confocal laser scanning microscope equipped with argon and HeNe laser with an excitation wavelength of 536 and 488 nm, respectively [48].

### 2.13. Scanning electron microscopy (SEM)

SEM (Scanning electron microscopy) was performed to analyze the morphology of preformed biofilm treated with curcumin-aPDT. The preformed biofilm was allowed to grown upon a glass coverslip in 6 well plate and treated as describe above. After treatment, biofilms in each sample (Control and treated) were fixed with 2% formaldehyde + 2.5% glutaraldehyde in PBS for 2 h at 4 °C. Different concentrations of ethanol (20%, 40%, 60%, 80%, and 100%) were used to dehydrate the fixed samples. The coverslips were dried, mounted and sputter coated with gold–palladium and analyzed under scanning electron microscope [48].

### 2.14. Cytotoxicity assay

A cytotoxicity assay was performed on human monocytic cell line THP1. The THP1 was cultured in ROSWELL PARK MEMORIAL INSTITUTE (RPMI) 1640, supplemented with 10% fetal bovine serum (FBS) and 1% antibiotic i.e. penicillin–streptomycin (pen-strep) at 37 °C, and 95% humidified incubator with 5% $CO_2$. Sterile conditions were maintained all the times. Cells (~$10^5$cells/well) were seeded in 96-well plates, left overnight to adhere (THP1 as a monocyte were differentiated into macrophages using PMA of stock solution 10 ng per μl and working solution of 20 ng per ml) cells were exposed to and then treated with various concentrations of curcumin (39 μg/ml, 78 μg/ml and 400 μg/ml) in the presence as well as in the absence of laser irradiation. After 24 h, cell survival was determined by a standard 3-(4,5-dimethyl thiazol-2-yl)-2,5-diphenyl tetrazolium bromide (MTT) assay. The supernatants were removed and 90 μl of fresh medium and 10 μl of MTT (1 mg/ml) solution were added to each well, followed by incubation for 4 h at 37 °C. The formazan crystals formed by the reduction of MTT were dissolved in 150 μl of DMSO and the absorbance was quantified by measuring its optical density at a wavelength of 570 nm using spectrophotometer [54].

### 2.15. Antimicrobial photodynamic therapy against VRSA induced topical infection in male wistar rats

#### 2.15.1. Rat model of skin abrasion

In the experiment, a total of 40 adult male wistar rats, weighing, 250–300 g, were used. The rats were divided into 2 main groups i.e. the normal group and the immunocompromised group. Each group consisted of 20 rats, which were further sub-divided into 4 groups of 5 rats each. Group 1 consisted of rats without infection (Control); Group 2 contained rats with infection (Untreated); Group 3 contained rats treated with only curcumin (78 μg/ml); Group 4 was rats treated with curcumin (78 μg/ml) + laser light (20 J/cm$^2$);

The animals were housed 5 per cage and kept on a 12-hour light/dark cycle with access food and water ad libitum. At day 1 and 4, rats were administered two doses of cyclophosphamide. The first dose was 150 mg cyclophosphamide per kg of rat body weight (150 mg/kg), injected intraperitoneally (i.p.) followed by the second dose of 100 mg/kg. This treatment reduced peripheral blood neutrophils to < 100/ml blood [45], fostering a more susceptible environment for infection in the rats. Before the creation of wounds, rats were anesthetized with i.p. injections of ketamine/xylazine cocktail and then shaved on the dorsal surfaces using 28-gauge needles. Skin abrasion wounds were made by creating 6 × 6 crossed scratch lines within a defined 1 × 1 cm$^2$ area [2,45].

#### 2.15.2. Infection induction

Five minutes after wounding, an aliquot of 50 μl suspension containing $10^8$ CFU of VRSA in PBS was inoculated over each defined area in normal and immunocompromised rats containing the crossed scratches with a pipette tip. They were observed carefully for symptoms of disease (weight, ruffled fur and inactivity) and rats that become moribund were sacrificed [55].

#### 2.15.3. Antimicrobial photodynamic therapy on vancomycin resistant Staphylococcus aureus (VRSA) infected wistar rats

All experiments using rats that had been treated with curcumin were carried out under subdued room lighting or in the dark, except when illumination was taking place. Curcumin was added at sub-MIC concentration (78 μg/ml) in the middle and spread over the whole infected area. Thirty minutes after the addition of curcumin, irradiation was carried out with 405 nm of laser light for 52 s which corresponds to 20 J/cm$^2$ [45].

#### 2.15.4. Effects of aPDT on the number of viable bacteria in the skin abrasion

In order to confirm the absence of VRSA colonization in the skin abrasion, bacterial load was measured for every sample by CFU counting on BHI agar plates and expressed as CFU per ml. Swab samples were taken from the infected skin surfaces of the rats after 24 h of the infection. Treatment was given after every 24 h for three weeks and then the samples from control and treated groups were serially diluted and plated on BHI agar plates for total cell counts. The plates were incubated at 37 °C for 24 h before enumeration of colonies of VRSA [56].

### 2.16. Histopathological analysis

Fresh skin biopsies of both control and aPDT treated rat groups were incised and fixed in 10% phosphate buffered formalin (pH 7.4). The tissues were then dehydrated in ascending grades of ethyl alcohol, cleared in xylene and mounted in molten paraplast at 58–62 °C. Serial 5-μm histological sections were cut and stained with haematoxylin and eosin (H/E) to examine microorganism response [57].

### 2.17. Effects of curcumin mediated aPDT on inflammatory markers

To determine the production level of cytokines, blood samples were drawn and collected into sterile blood collection tubes from the eyes of controls, untreated, only curcumin treated and curcumin with light treated groups of normal and immunocompromised rats under anesthesia. Thereafter, all rats were immediately sacrificed as per the guidelines. The blood samples were centrifuged at 5000 rpm for 5 min. After centrifugation, the serum supernatant was aliquoted in microcentrifuge tubes and stored at −80 °C for further analysis [58].The commercially available enzyme-linked immunosorbent assay (ELISA) kits were used according to the manufacturers' protocol: Rat TNFα ELISA Kit (RAY BIOTECH, CAT: ELR-TNFA), Rat IL-6 ELISA Kit (RAY BIOTECH, CAT: ELR-IL6). The levels of TNF-α and IL-6 were measured by ELISA reader (BIORAD MICROPLATE READER, INDIA).

### 2.18. Statistical analysis

All data were presented as averages of the values obtained ± S.D. of three independent experiments. Test groups were compared with the control group using the Student's *t*-test. Free online software, one-way analysis of variance (ANOVA) [59] was used for the comparison of multiple means. For in vivo experiments, all the results were expressed as mean ± S.D. for five rats in each group. Data with $P \leq \alpha = 0.05$ and $P < \alpha = 0.01$ were considered to be statistically significant (following the confidence level of 95%).

## 3. Results

### 3.1. Antimicrobial susceptibility

The isolated strain of *Staphylococcus aureus* was found to be highly resistant against vancomycin (Supplementary figure S1).

### 3.2. Bacteria susceptibility assay

The MIC and MBC of curcumin in the presence as well as in the absence of laser irradiation against VRSA is shown in Table 1.The MIC value of curcumin-aPDT for VRSA was found to be 156.25 μg/ml whereas sub-MIC (1/2 of MIC) was found to be 78 μg/ml. Sub-minimum inhibitory concentration (sub-MIC) of curcumin (78 μg/ml = 1/2 of MIC) was taken as a standard to evaluate the antimicrobial and antibiofilm effect of curcumin mediated photodynamic therapy against vancomycin resistant *Staphylococcus aureus* (VRSA).

### 3.3. Enhanced production of intracellular ROS

The result showed 4.8fold increase in DCF fluorescence intensity in only curcumin treated group. While 5.8 fold increase in the DCF fluorescence was observed when the cells were treated with curcumin followed by laser irradiation at a concentration of 78 μg/ml as compared to control group. This data clearly proved that more ROS were produced in curcumin-aPDT treated group than curcumin alone. Whereas, no ROS production was seen in the group treated with light only. Hence, for

**Table 1**
Determination of minimum inhibitory concentration (MIC) and minimum bactericidal concentration (MBC) concentration of curcumin against Vancomycin resistant *Staphylococcus aureus* (VRSA).

| Strain : Vancomycin resistant *Staphylococcus aureus* (VRSA) | | | | |
|---|---|---|---|---|
| S. No. | Treatment | Minimum inhibitory concentration (MIC) in μg/ml | Sub-MIC (1/2 of MIC) in μg/ml | Minimum bactericidal concentration (MBC) in μg/ml |
| 1. | **Only Curcumin** | 5000 | 2500 | >5000 |
| 2. | **Curcumin + light(20 J/cm$^2$ = 52 s)** | 156.25 | 78 | 312.5 |

further study, only curcumin and curcumin with light treated groups were selected (Fig. 1).

### 3.4. Quenching of hydroxyl radical

HPF probe was used to determine ˙OH radicals formed by curcumin mediated aPDT in order to check if type I ROS generated. This data revealed that curcumin-aPDT caused quenching of ˙OH radicals (Fig. 2A). It is evident from the results that more quenching of hydroxyl radical was observed in curcumin without light as compared to curcumin with light treatment. Since, laser treatment reduces the quenching effect of curcumin, therefore same concentration of curcumin with light shows less quenching as compared to curcumin without light.

### 3.5. Elevated production of singlet oxygen

The $^1O_2$ production abilities of curcumin were also quantified in PBS by measuring the degradation rate of AMDA. Enhanced $^1O_2$ quantum yield was observed at sub-MIC of curcumin followed by light irradiation as compared to only curcumin treated group (Fig. 2B). Since, the amount of ROS produced is directly proportional to the bacterial cell death; curcumin without light treated group shows less $^1O_2$ production than curcumin with light irradiation. This confirmed that type II photochemistry is the major photochemical reaction involved in curcumin mediated aPDT.

### 3.6. Bacterial load reduction (CFU/ml)

A significant 3.05 $\log_{10}$ reduction in bacterial load was observed when preformed biofilm of VRSA was exposed to curcumin at sub-MIC (78 μg/ml) concentration and subsequently to 20 J/cm$^2$ of laser irradiation, which corresponds to 52 s. Whereas only 1.19 $\log_{10}$ reduction was found in the group treated with only curcumin (Fig. 3).

### 3.7. Reduction of VRSA biofilm when treated with curcumin mediated aPDT

The effect of curcumin mediated aPDT on preformed biofilm of VRSA is shown in Fig. 4A. A 37.32% of biofilm reduction was observed in only curcumin (78 μg/ml) treated group while, approximately, 67.73% reduction in biofilm was found in curcumin with light treated group, as compared to control.

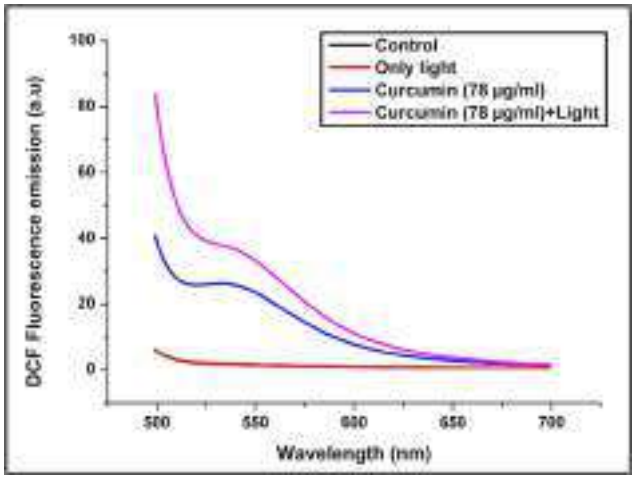


**Fig. 1.** Detection of total reactive oxygen species in VRSA by fluorescence intensity of 2′,7′-dichlorofluorescein (DCF) after curcumin mediated aPDT with 20 J/cm$^2$ of light irradiation. Control represents without any treatment.

### 3.8. Decrease level of EPS upon curcumin mediated aPDT

EPS formation is essential for the structure of biofilm, its spread and maintenance. The level of EPS was estimated by congo-red binding assay, which directly measures the relative amount of EPS after aPDT. A significant decrease in EPS level was detected in VRSA in the presence of curcumin followed by light irradiation (Fig. 4B). 47.94% EPS reduction was observed with sub-MIC (78 μg/ml) concentration of curcumin with light, whereas 13.66% reduction was found in only curcumin treated group. The highest EPS level was seen in the control group without any treatment.

### 3.9. Impairment of biofilm architecture visualized through confocal microscopy

CLSM analysis was performed to check the consequence of aPDT on the viability of VRSA biofilm. In control group, lawn of green fluorescing VRSA cells were shown, indicating all live cells (Fig. 5A). Cells treated with only curcumin, showed both green (live) and red (dead) fluorescence as shown in Fig. 5B. However, most prominent reduction was seen in aPDT treated group. Majority of the cells were dead throughout the biofilm at 78 μg/ml of concentration of curcumin with 20 J/cm$^2$ of blue laser light treatment as shown in Fig. 5C.

### 3.10. SEM analysis of VRSA biofilm architecture

SEM analysis was carried out to elucidate the overall morphology of the cells in the biofilm after aPDT. Cells in the control group (Fig. 5D) were embedded in an EPS matrix that accelerates cell clustering. Remarkable reduction was found in the number of adherent bacteria upon treatment of biofilm with 78 μg/ml (Fig. 5F) concentration of curcumin along with light irradiation, as compared to only curcumin treated (Fig. 5E) group. Furthermore, cells in aPDT treated groups were completely ruptured, became irregularly shaped and showed leakage of cellular constituents (Fig. 5F, enlarged image of curcumin + light treated VRSA biofilm is provided in the supplementary information; figure S4).

### 3.11. Cytotoxicity of curcumin mediated aPDT on human monocytic cell line THP1

The cytotoxic effect of curcumin mediated aPDT was evaluated by MTT assay. The relative cellular viability of human monocytic cell line THP1 in the presence of different concentrations (39 μg/ml, 78 μg/ml and 400 μg/ml) of curcumin with and without light irradiation is shown in Fig. 6. Almost 52% viability was observed at a concentration of 400 μg/ml as compared to that used in this study. Thus, the test concentration of curcumin (78 μg/ml) with light treatment (20 J/cm$^2$ = 52 s) was found nontoxic to THP1 cell line.

### 3.12. In vivo experiments

#### 3.12.1. Curcumin mediated anti-microbial photodynamic therapy reduces bacterial load in normal and immunocompromised rat model of VRSA skin infection

Bacterial load was measured by CFU counting on BHI agar plates (Supplementary figure S3). The weekly recovery of rats over 3 weeks post treatment is shown in Fig. 7. The effects of photosensitization of curcumin demonstrated significant reduction in the bio-burden of VRSA in immunocompromised rats, which would otherwise develop severe infections. Curcumin-aPDT treated groups showed complete eradication of VRSA as compared to infection control group (Fig. 8). After 24 h of infection in immunocompromised rats, we found 2.7 $\log_{10}$ and 4 $\log_{10}$ reduction in only curcumin and curcumin with light treated groups, respectively, as compared to its untreated group. While in normal rats, we found 2.2 $\log_{10}$ and 3.8 $\log_{10}$ reduction in only curcumin and

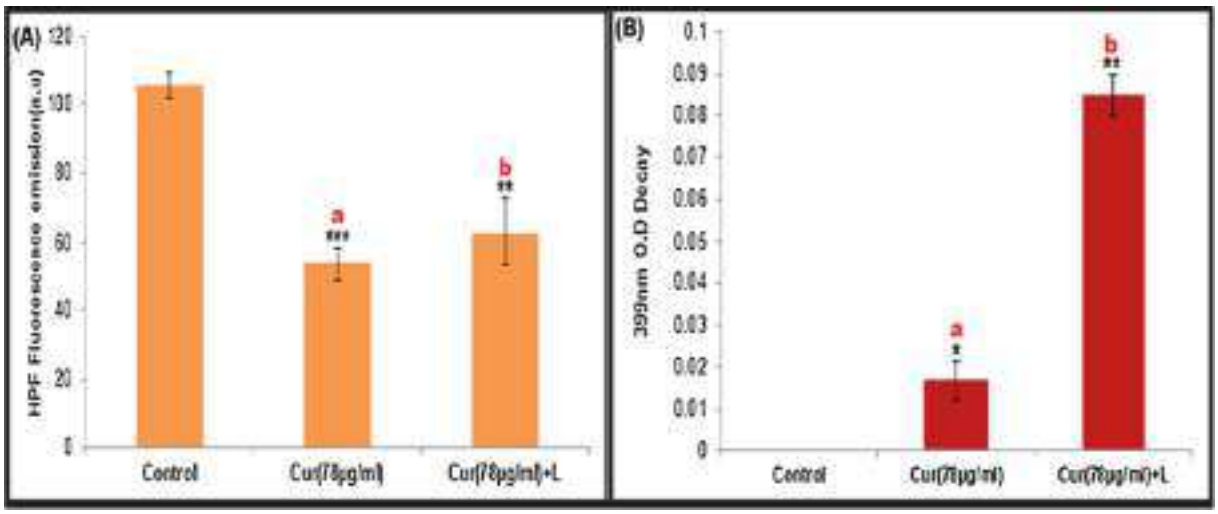


**Fig. 2.** Mechanism of aPDT: (A) Detection of ˙OH radical (Type I) after 20 J/cm$^2$ light irradiation by HPF fluorescence probe. (B) Quantification of singlet oxygen (Type II) by AMDA under 20 J/cm$^2$ of light irradiation. Data are presented as mean ± SD (n = 3). Test groups were compared with the control group using the Student's *t*-test and one-way analysis of variance (ANOVA) was used for the comparison of multiple means. Data with p-value of<0.05 (*p < 0.01, **p < 0.001, ***p < 0.0001) was considered statistically significant. a - Only curcumin treated group compared with control or untreated group; b - Curcumin + light treated group compared with control or untreated group.

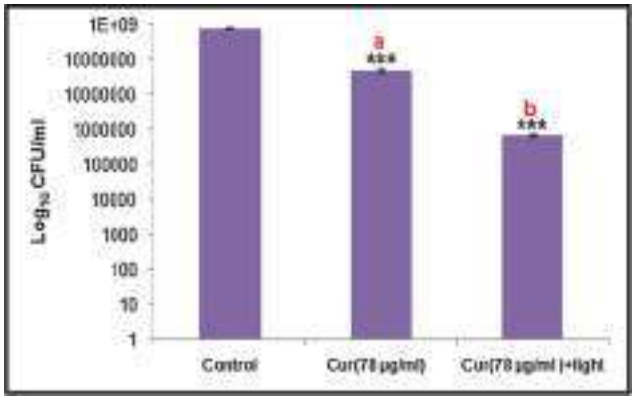


**Fig. 3.** Effect of aPDT on preformed vancomycin resistant *Staphylococcus aureus* (VRSA) biofilm: Preformed biofilm of VRSA was incubated with curcumin (78 µg/ml) followed by exposure to 20 J/cm$^2$ of light. Control represent without curcumin and light treatment. Data are presented as mean ± SD (n = 3). Test groups were compared with the control group using the Student's *t*-test and one-way analysis of variance (ANOVA) was used for the comparison of multiple means. Data with p-value of<0.05 (*p < 0.01, **p < 0.001, ***p < 0.0001) was considered statistically significant. a - Only curcumin treated group compared with control or untreated group; b - Curcumin + light treated group compared with control or untreated group.

curcumin with light treated group, respectively. In immunocompromised rats, reduction in bacterial counts after three weeks was found to be 3.2 $\log_{10}$ in only curcumin treated group. Whereas, in curcumin with light treated group almost complete eradication of bacterial load was observed. Curcumin with light treated group in normal rats showed complete recovery of skin abrasion as compared to its untreated group, which may be due to its innate immunity.

### 3.12.2. Histopathological observations

An expert pathologist did histopathological evaluations of the biopsy samples of rat skin. Haematoxylin and eosin stained sections of normal untreated rats showed the prevalence of focal lesions in the dermis with dense neutrophilic infiltrate. Acute inflammatory cells were dispersed around skin adnexa whereas immunocompromised untreated rats exhibited focally atrophied epidermis and hyperkeratosis with focal, dense neutrophilic infiltrate in the epidermis and dermis extending to the deeper muscle fibres. Curcumin-aPDT treated normal rats showed atrophied stratified squamous epithelial cell with hyperkeratosis and sparsely dispersed neutrophilic infiltrate in the dermis. Focal atrophied ducts were also seen in the dermis while in immunocompromise rats, focally acanthotic stratified squamous epithelial cells with mild neutrophilic infiltrate in the papillary dermis and sparsely distributed inflammatory cells around the sebaceous glands were observed. In other treated sample (those which were treated with only curcumin), a moderate neutrophilic infiltrate was observed throughout epidermal, dermal and papillary dermal layers (Fig. 9).

### 3.12.3. Anti-inflammatory activity of curcumin followed by exposure of blue laser light in a rat model of skin abrasion

After the rats were sacrificed, two types of pro-inflammatory cytokines tumor necrosis factor-α (TNF-α) and interleukin-6 (IL-6) were measured in the serum sample to evaluate the degree of inflammation. It was found that skin abrasion infected with VRSA, in both normal and immunocompromised rats has led to a significant increase in TNF-α and IL-6 levels ($p < 0.05$). However, decreased levels of cytokines were produced in normal rat groups after infection as compared to immunocompromised group implying suppression of immune activities by cyclophosphamide.

In immunocompromised rats, the effective treatment dose of curcumin alone leads to substantial decrease in the production levels of these pro-inflammatory cytokines when compared with untreated group. However, remarkable decrease in IL-6 and TNF-α level was found in curcumin-aPDT treated group. The level of cytokines in normal rats was also found to be reduced after curcumin-aPDT treatment (Fig. 10). The obtained result showed that sub-MIC (78 µg/ml) concentration of curcumin on exposure to 20 J/cm$^2$ of blue laser light restores immunosuppression and surges immunity by augmenting the productions of cytokines.

## 4. Discussion

The growing resistance in pathogenic bacteria against existing antibiotic remains a major concern for public health. *Staphylococcus aureus* infections represent a growing proportion of severe community-acquired and nosocomial infections [60–63]. Majority of these infections are now being caused by multidrug-resistant strains, including

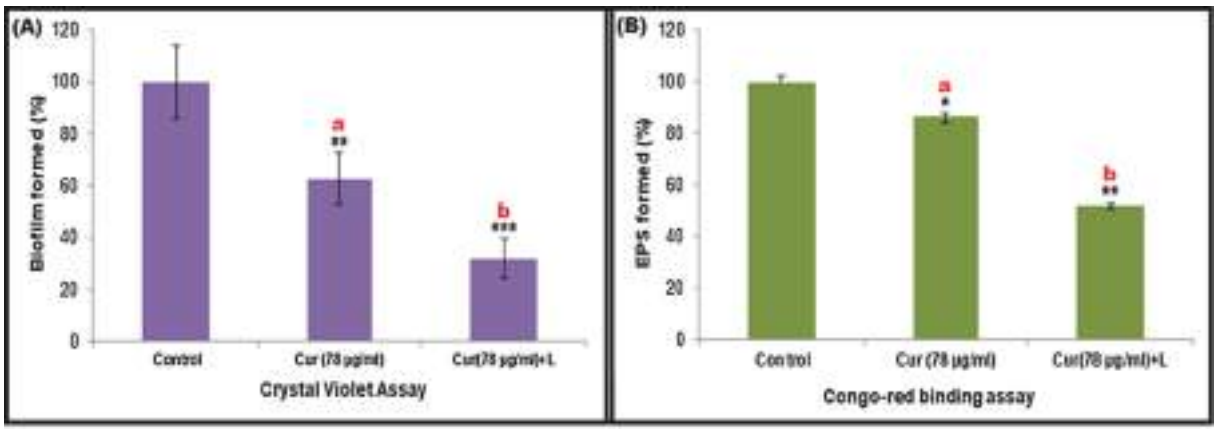


**Fig. 4.** (A) Inhibitory effect of curcumin mediated aPDT on preformed biofilm of VRSA quantified by Crystal violet assay. Absorbance was measured at 630 nm. (B) Congo-red assay: effect of curcumin mediated aPDT on extracellular polysaccharide substance (EPS) reduction. Absorbance was measured at 490 nm. Data are presented as mean ± SD (n = 3). Test groups were compared with the control group using the Student's *t*-test and one-way analysis of variance (ANOVA) was used for the comparison of multiple means. Data with p-value of<0.05 (*p < 0.01, **p < 0.001, ***p < 0.0001) was considered statistically significant. a - Only curcumin treated group compared with control or untreated group; b - Curcumin + light treated group compared with control or untreated group.

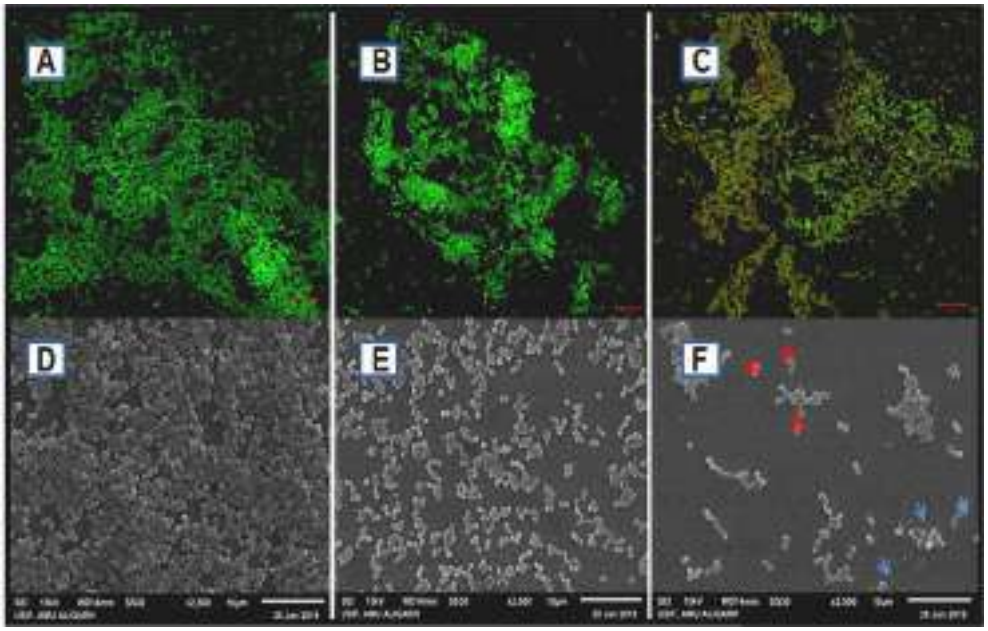


**Fig. 5. Live/dead fluorescent staining images of VRSA biofilm:** (A) Control biofilm, (B) Only curcumin (78 µg/ml) (C) Curcumin (78 µg/ml) + light. The images represent bacterial biofilm cells stained with SYTO 9 (green/live) and PI (red/dead). Scale bar = 10 µm. **Biofilm Assessment and Structural Imaging:** Scanning electron microscopy (SEM) images of VRSA biofilm. (D) Control biofilm, (E) Only curcumin (78 µg/ml) (F) Curcumin (78 µg/ml) + Light. Red arrow indicates bursting and release of cellular constituents while blue arrow indicates complete rupturing of the cells. (For interpretation of the references to colour in this figure legend, the reader is referred to the web version of this article.)

vancomycin or methicillin resistant *S. aureus* [64–67]. In such situation, when no antibiotic is left to treat, antimicrobial photodynamic therapy can be used as an alternative approach. When compared with other antimicrobial therapies, aPDT has several advantages such as absence of long-term toxicity, ability to kill microorganisms in a very less time and high repeatability without developing resistance [23,68]. Several studies have been reported depicting the efficacy of antimicrobial photodynamic therapy with various photosensitizers against *S. aureus* [69–71]. In the present study; we have examined the antimicrobial effect of curcumin-mediated aPDT against preformed biofilm of VRSA, through in vitro and in vivo experiments.

Curcumin mediated antimicrobial photodynamic therapy was proved to be highly effective in eliminating vancomycin resistant *Staphylococcus aureus* (VRSA) biofilm. Earlier studies on planktonic *S. aureus* have shown that curcumin activity is significantly improved in the presence of blue LED light irradiation at the wavelength of 470 nm [44].

Preliminary in vitro studies of curcumin mediated aPDT against VRSA were carried out with MIC and MBC, wherein MIC and MBC of only curcumin treated group were found to be 5000 µg/ml and > 5000 µg/ml, respectively, as compared to MIC and MBC of curcumin with light treated group (156.25 µg/ml and 312.5 µg/ml, respectively) (Table. 1). Considering the cytotoxic effects of curcumin on human cells followed by laser irradiation, THP-1 cells were exposed to different concentrations (39 µg/ml, 78 µg/ml and 400 µg/ml) of curcumin. Even at a higher concentration (400 µg/ml), the cellular viability of curcumin along with light irradiation was found to be>52% after 24 h of incubation as observed in MTT assay (Fig. 6). Hence, the concentration and exposure time of blue laser light used in this study was found to be non-toxic.

Curcumin mediated antimicrobial photodynamic therapy possesses dual properties such as the direct antibacterial activity of curcumin itself as well as its ROS-mediated effect upon blue light irradiation [44]. In antimicrobial photodynamic therapy, killing or cellular damage is directly proportional to the amount of ROS produced. Therefore, we have checked total intracellular ROS generation by DCFH-DA. An

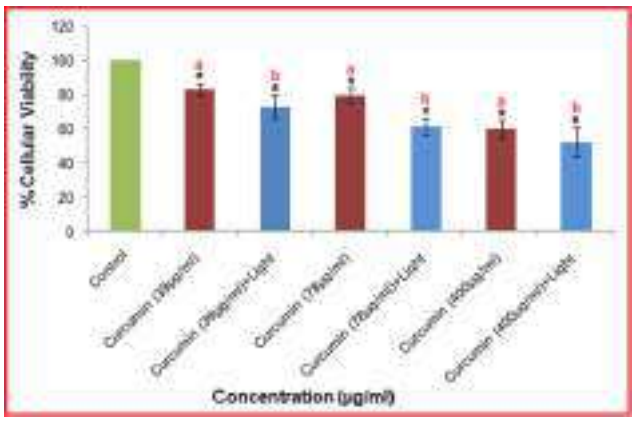


**Fig. 6.** MTT assay: Cytotoxicity of curcumin mediated aPDT on human monocytic cell line (THP1). Data are presented as mean ± SD (n = 3). Test groups were compared with the control group using the Student's *t*-test and one-way analysis of variance (ANOVA) was used for the comparison of multiple means. Data with p-value of<0.05 (*p < 0.01, **p < 0.001, ***p < 0.0001) was considered statistically significant. a - Only curcumin treated group compared with control or untreated group; b - Curcumin + light treated group compared with control or untreated group.

esterase enzyme causes hydrolysis of DCFH-DA to DCFH, which is further oxidized in the presence of ROS to produce a fluorescent compound DCF. Our data showed significant increase in the intracellular ROS production in curcumin-aPDT treated group as compared to those treated with curcumin alone (Fig. 1) which is in accordance with the data obtained by Jiang *et al.*, 2014, who has demonstrated that, blue light activated curcumin, causing excessive accumulation of intracellular ROS, leads to loss of VRSA cells.

The mechanism of action involved in antimicrobial photodynamic therapy is merely dependent upon the ability of a photosensitizer to generate ROS such as free radical ($HO^{\bullet}$, $H_2O_2$ and $O_2^{\bullet-}$ via type I mechanism) and $^1O_2$ (via type II mechanism), when irradiated with light. In order to check the presence of $HO^{\bullet}$ (Type I photochemistry), we have used HPF fluorescence compound, specific for the quantification of hydroxyl radical. Our data showed fluorescence quenching in the group treated with curcumin (78 µg/ml) alone as compared to curcumin-aPDT treated group (Fig. 2A). Hence, we further quantify the production of singlet oxygen (Type II photochemistry). We have used AMDA which shows three distinctive absorption bands at 399 nm, 378 nm and 359 nm. The decrease in the absorption at 399 nm is proportional to the amount of $^1O_2$ being produced [72].Our data showed higher amount of $^1O_2$ generation in curcumin mediated aPDT treated group as compared to curcumin alone(Fig. 2B). This confirms that singlet oxygen ($^1O_2$) causes detrimental effects on VRSA cells as compared to hydroxyl radicals. The bacterial cell have sufficient amount of scavengers such as catalase, peroxidase and superoxide dismutase to thwart the free radical mediated bactericidal activity, however they have no remedy against the singlet oxygen molecule, as a result, $^1O_2$ leads to maximum cell damage [73]. Biofilms forming bacteria are difficult to treat, since it protects the microorganisms from antibiotics and other antimicrobial agents leading to develop drug resistance [50,74–75].One of the most pathogenic biofilm-forming bacteria is *Staphylococcus aureus*. In the present study, we have examined whether curcumin mediated aPDT affects preformed biofilm of VRSA. Fig. 3 shows that curcumin-aPDT significantly reduced preformed biofilm of VRSA at a concentration of 78 µg/ml of curcumin and 20 J/cm$^2$ laser irradiation which correspond to 52 s. 3.05 $\log_{10}$ reduction was observed in curcumin-aPDT treated group as compared to 1.19 $\log_{10}$ reduction in only curcumin treated

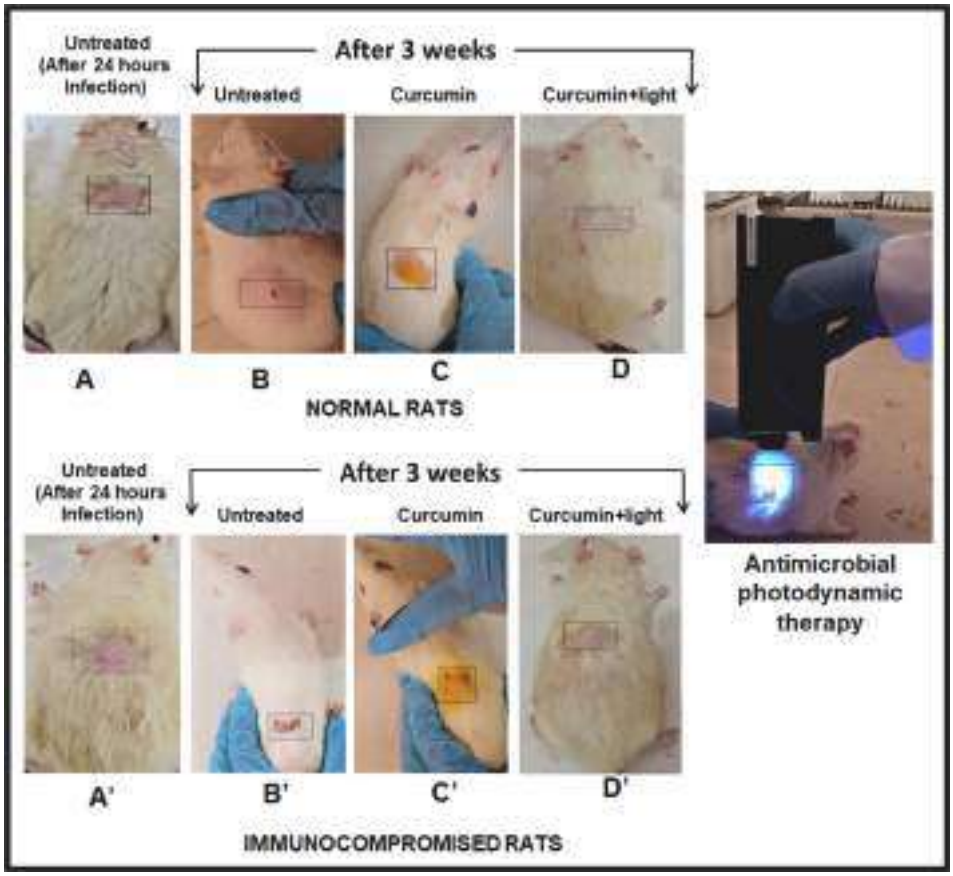


**Fig. 7.** Male wistar rat model of skin abrasion and its treatment.

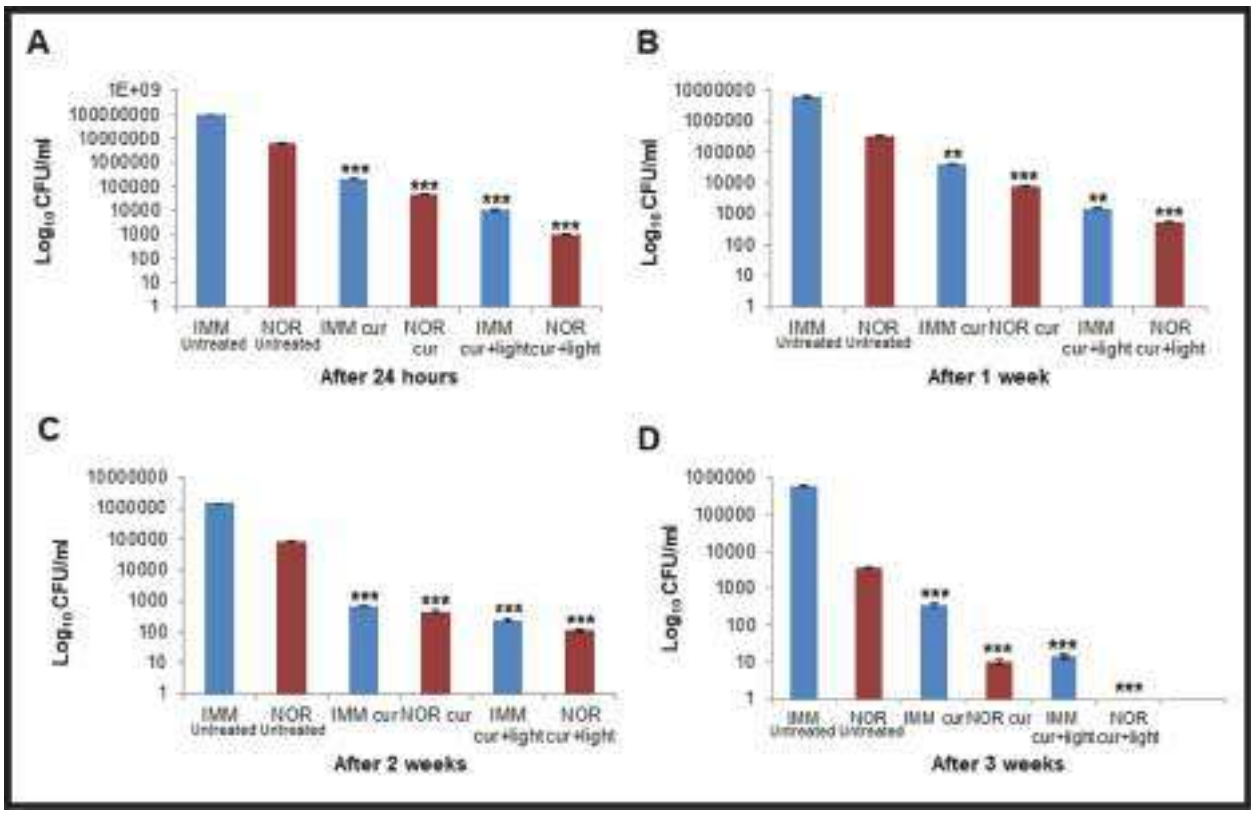


**Fig. 8.** Bacterial load reduction in normal and immunocompromised male wistar rats. (A) CFU/ml after 24 h of post infection, (B) CFU/ml after 1 week of post infection and treatment, (C) CFU/ml after 2 weeks of post infection and treatment and (D) CFU/ml after 3 weeks of post infection and treatment. IMM untreated: immunocompromised untreated rats; NOR untreated: normal untreated rats; IMM cur: immunocompromised rats treated with curcumin only; NOR cur: normal rats treated with curcumin only; IMM cur + light: immunocompromised rats treated with curcumin followed by 20 J/cm$^2$ of light treatment; NOR cur + light: normal rats treated with curcumin followed by 20 J/cm$^2$ of light treatment. Data are presented as mean ± SD (n = 5). Test groups were compared with the control group using the Student's *t*-test and one-way analysis of variance (ANOVA) was used for the comparison of multiple means. Data with p-value of<0.05 (*p < 0.01, **p < 0.001, ***p < 0.0001) was considered statistically significant.

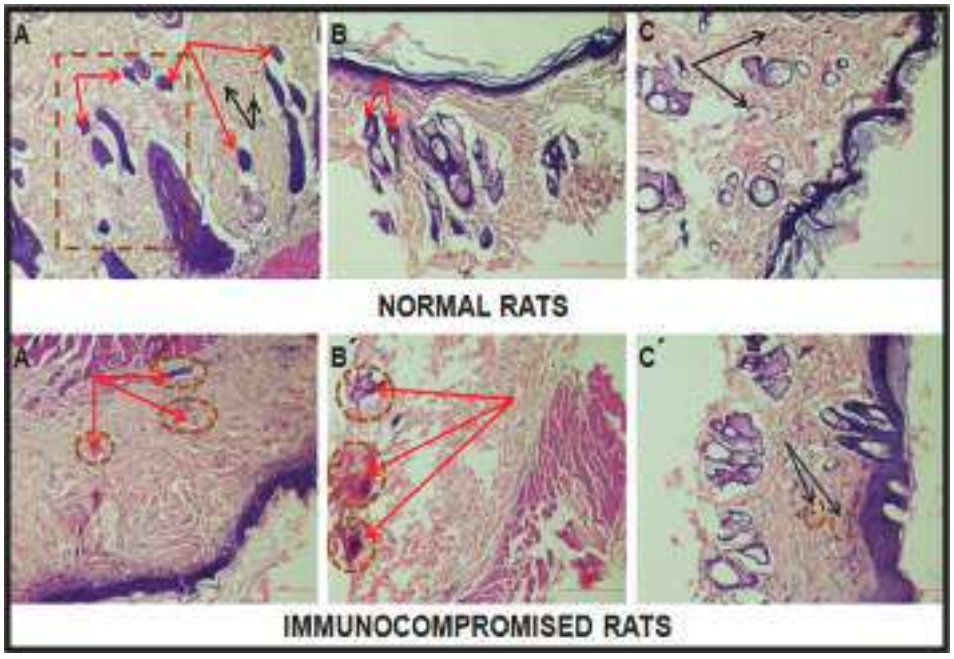


**Fig. 9.** Histopathological investigation by haematoxylin and eosin (H/E) staining to examine response to microorganism. Scale bar = 500 μm. Normal rats: (A) Untreated, (B) Only curcumin treated and (C) Curcumin + Light treated. Immunocompromised rats: (A′) Untreated, (B′) only curcumin treated and (C′) Curcumin + light treated groups respectively. Untreated: rats without any treatment after 3 weeks of post infection. Note: Brown dashed line indicates site of infection. Red arrow indicates focal dense neutrophilic infiltrate, black arrow indicates dispersed or scattered neutrophilic infiltrate while blue arrow indicates mild neutrophilic infiltrate. (For interpretation of the references to colour in this figure legend, the reader is referred to the web version of this article.)

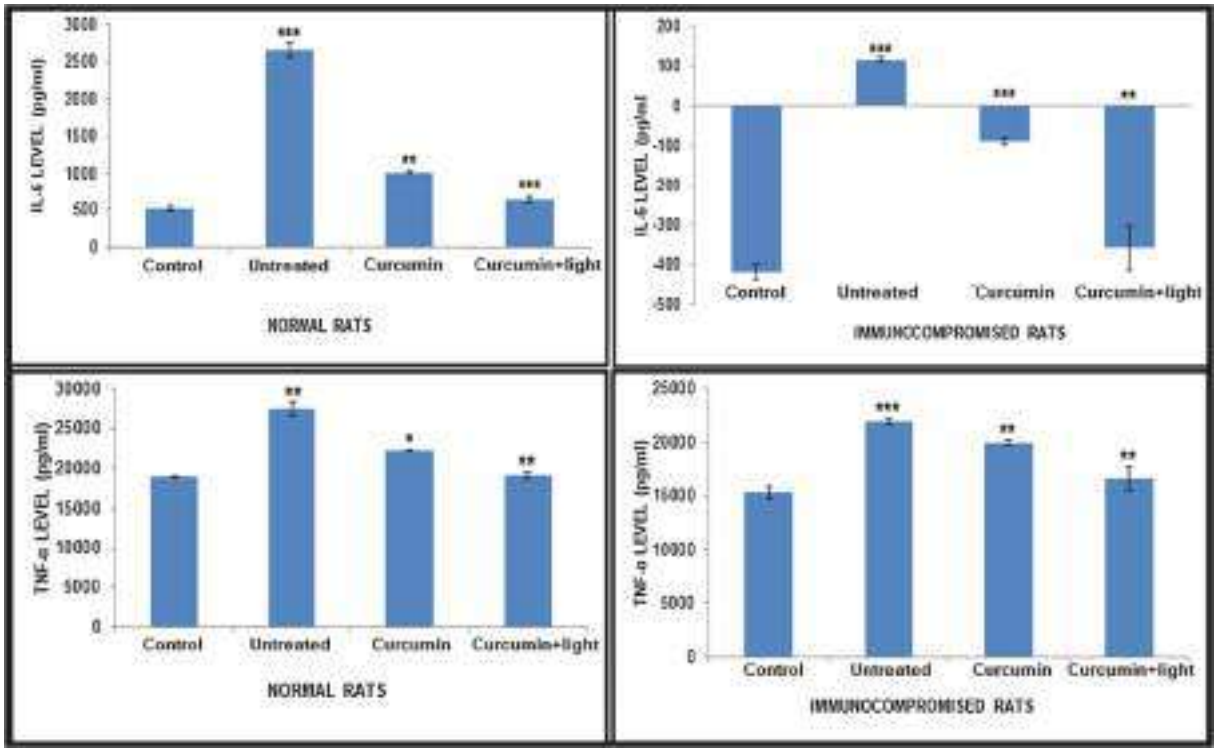


**Fig. 10.** Anti-inflammatory effects of curcumin mediated aPDT in a rat model of Skin abrasion. Normal rats: (A) Level of IL-6 and (B) Level of TNF-α. Immunocompromised rats: (A′) Level of IL6 and (B′) Level of TNF-α respectively. Data are presented as mean ± SD (n = 5). Test groups were compared with the control group using the Student's *t*-test and one-way analysis of variance (ANOVA) was used for the comparison of multiple means. Data with p-value of<0.05 (*p < 0.01, **p < 0.001, ***p < 0.0001) was considered statistically significant.

group. This shows that curcumin mediated aPDT could be sufficient to inhibit biofilm forming VRSA.

Curcumin mediated aPDT results in reduced microbial biomasses as well as EPS production which are of considerable importance for the construction of biofilm architecture [76]. Reduction in biofilm formation was found to be 37.32% in the presence of curcumin, whereas, 67.73% reduction was observed at sub-MIC (78 μg/ml) of curcumin with light irradiation, as compared to control (Fig. 4A). EPS reduction at sub-MIC (78 μg/ml) concentration of curcumin with light was found to be 47.94%, whereas 13.66% reduction was observed in only curcumin treated group as evaluated by Congo red assays (Fig. 4B).

Furthermore, XTT assay was performed to determine the number of viable cells present after aPDT treatment. Reduced viability was seen when preformed biofilm of VRSA was treated with curcumin mediated aPDT as compared to curcumin alone. Our data revealed that majority of the cells in the biofilm were found to be metabolically active but unable to form a biofilm. This may be due to the inhibitory action of curcumin mediated aPDT (Supplementary figure S2).

Microscopic studies revealed that curcumin mediated aPDT altered the phenotype of the VRSA biofilm. CLSM micrographs illustrate greater disruption of biofilm architecture in curcumin-aPDT treated groups i.e., many bacterial cells were found to be dead (red) within the preformed biofilm of VRSA (Fig. 5C). Thereby demonstrating curcumin-aPDT exhibits strong antimicrobial action against VRSA biofilm. This observation was further supported by the scanning electron microscopy. Unlike the untreated cells (Fig. 5D), with larger cellular aggregates, the treated cells showed detrimental effects on cell wall with significant dispersion of the cells leading to leakage of the cellular content, thus obliterating the structural integrity of a biofilm (Fig. 5F).

We have also examined the effect of curcumin mediated aPDT in rat model of skin abrasion. The result showed daily topical exposure of curcumin followed by light irradiation led to marked reduction of VRSA in normal as well as in immunocompromised rats (Figs. 7 and 8). This finding is supported by previous study where pronounced reduction in soft-tissue infection with methicillin-resistant *S. aureus* (MRSA), has been observed after aPDT treatment [55].In addition, the result of histopathological investigation represents complete bacterial clearance with no visible bacterial colonies in curcumin-aPDT treated wound of normal and immunocompromised rats (Fig. 9) [56]. Furthermore, we have checked the immune-protective role of curcumin-aPDT in infection control by proinflammatory cytokines (TNF-α and IL-6) profiling. Cytokines are the soluble glycoproteins possessing several immune functions [77]. Th1 and Th2 cells are the two main subsets of $CD4^+$ T helper cells. Both the cells maintain a relatively balanced state and secrete different types of cytokines. However, any disturbances in Th1 and Th2 immune responses lead to various diseases. Th1 immune responses induce inflammatory bowel diseases [78], while Th2 immune responses are associated with atopic diseases [79]. In our study, the level of cytokines in normal rats as well as in immunocompromised rats was found to be reduced dramatically after curcumin-aPDT treatment. Furthermore, our results showed that curcumin mediated aPDT restores immunosuppression and improves immunity by augmenting the production of cytokines (Fig. 10).

## 5. Conclusions

This is the first time we have successfully cured VRSA induced skin infection, both in normal and immunocompromised wistar rats using curcumin mediated aPDT. Hence, we proposed that curcumin mediated aPDT could be used against multi-drug resistant bacterial infections and preformed biofilm formation as a potential therapeutic approach (Graphical abstract).

## Declaration of Competing Interest

The authors declare that they have no known competing financial

interests or personal relationships that could have appeared to influence the work reported in this paper.

*Acknowledgements*

We are grateful to Dr. Dhiraj Kumar and Dr. Varthika Sharma, Cellular Immunology group, ICGEB, New Delhi, for providing cell culture facilities. We acknowledge Professor Shabbir Ahmed, Department of Physics, AMU, for providing laser. The authors would also like to acknowledge university sophisticated instruments facility (USIF), AMU, for providing instrumental support.

*Funding*

This work was supported by Department of Science and Technology Research grant, DST: SR/NM/NS-41/2016(G). FA acknowledged fellowship from Council of Scientific and industrial research: 09/112 (0600)/2018-EMR-I.

## Appendix A. Supplementary data

Supplementary data to this article can be found online at https://doi.org/10.1016/j.ejpb.2021.01.012.

## References

[1] S. Hasan, S.Z. Ali, A.U. Khan, Novel combinations of antibiotics to inhibit extended spectrum β-lactamase and metallo-β-lactamase producers in vitro: a synergistic approach, Future Microbiol. 8 (2013) 939–944.
[2] M. Krishnamurthy, M.M. Lemmon, E.M. Falcinelli, R.A. Sandy, J.N. Dootz, T. M. Mott, S. Rajamani, K.E. Schaecher, A.J. Duplantier, R.G. Panchal, Enhancing the antibacterial activity of polymyxins using a nonantibiotic drug, Infect. Drug Resist. 12 (2019) 1393–1405.
[3] L.M. de Freitas, E.N. Lorenzón, N.A. Santos-Filho, L.H.d.P. Zago, M.P. Uliana, K.T. de Oliveira, E.M. Cilli, C.R. Fontana, Antimicrobial Photodynamic therapy enhanced by the peptide aurein 1.2, Scient. Reports, 8 (2018).
[4] S. Khan, S.N. Khan, F. Akhtar, L. Misba, R. Meena, A.U. Khan, Inhibition of multi-drug resistant Klebsiella pneumoniae: Nanoparticles induced photoinactivation in presence of efflux pump inhibitor, Eur. J. Pharm. Biopharm. 157 (2020) 165–174.
[5] Q.Q. Yang, A.K. Farha, G. Kim, K. Gul, R.Y. Gan, H. Corke, Antimicrobial and anticancer applications and related mechanisms of curcumin-mediated photodynamic treatments, Trends Food Sci. Technol. 97 (2020) 341–354.
[6] H. Chen, H. Deng, X. Zou, J. Zhao, Hypocrellin B Encapsulated in Triphenyl Phosphonium-Modified Cationic Liposomes for Photodynamic Treatment of Exudative Age-Related Macular Degeneration, J. Biomed. Nanotechnol. 15 (2019) 2305–2320.
[7] Ursula Schmidt-Erfurth, Tayyaba Hasan, Mechanisms of action of photodynamic therapy with verteporfin for the treatment of age-related macular degeneration, Surv. Ophthalmol. 45 (3) (2000) 195–214.
[8] M. Gallardo-Villagrán, D.Y. Leger, B. Liagre, B. Therrien, Photosensitizers Used in the Photodynamic Therapy of Rheumatoid Arthritis, Int. J. Mol. Sci. 20 (2019) 3339.
[9] M.A.A. Freitas, A.H.C. Pereira, J.G. Pinto, A. Casas, J. Ferreira-Strixino, Bacterial viability after antimicrobial photodynamic therapy with curcumin on multiresistant Staphylococcus aureus, Future Microbiol. 14 (2019) 739–748.
[10] Y. Panahi, O. Fazlolahzadeh, S.L. Atkin, M. Majeed, A.E. Butler, T.P. Johnston, A. Sahebkar, Evidence of curcumin and curcumin analogue effects in skin diseases: A narrative review, J. Cell. Physiol. 234 (2018) 1165–1178.
[11] T.M. Branco, N.C. Valério, V.I.R. Jesus, C.J. Dias, M.G.P.M.S. Neves, M.A. F. Faustino, A. Almeida, Single and combined effects of photodynamic therapy and antibiotics to inactivate Staphylococcus aureus on skin, Photodiagn. Photodyn. Ther. 21 (2018) 285–293.
[12] W. Kałas, E. Wysokińska, M. Przybyło, M. Langner, A. Ulatowska-Jarża, D. Biały, M. Wawrzyńska, E. Zioło, W. Gil, A.M. Trzeciak, H. Podbielska, M. Kopaczyńska, Photoactive Liposomal Formulation of PVP-Conjugated Chlorin e6 for Photodynamic Reduction of Atherosclerotic Plaque, Int. J. Mol. Sci. 20 (2019) 3852.
[13] L. Costa, M.A.F. Faustino, J.P.C. Tomé, M.G.P.M.S. Neves, A.C. Tomé, J.A. S. Cavaleiro, Â. Cunha, A. Almeida, Involvement of type I and type II mechanisms on the photoinactivation of non-enveloped DNA and RNA bacteriophages, J. Photochem. Photobiol., B 120 (2013) 10–16.
[14] C.M.B. Carvalho, A.T.P.C. Gomes, S.C.D. Fernandes, A.C.B. Prata, M.A. Almeida, M. A. Cunha, J.P.C. Tomé, M.A.F. Faustino, M.G.P.M.S. Neves, A.C. Tomé, J.A. S. Cavaleiro, Z. Lin, J.P. Rainho, J. Rocha, Photoinactivation of bacteria in wastewater by porphyrins: Bacterial β-galactosidase activity and leucine-uptake as methods to monitor the process, J. Photochem. Photobiol., B 88 (2007) 112–118.
[15] A. Almeida, M.A.F. Faustino, J.P.C. Tomé, Photodynamic inactivation of bacteria: finding the effective targets, Future Med. Chem. 7 (2015) 1221–1224.
[16] M.R. Hamblin, T. Hasan, Photodynamic therapy: a new antimicrobial approach to infectious disease? Photochem. Photobiol. Sci. 3 (5) (2015) 436–450.
[17] L. Costa, M.A.F. Faustino, M.G.P.M.S. Neves, Â. Cunha, A. Almeida, Photodynamic Inactivation of Mammalian Viruses and Bacteriophages, Viruses 4 (2012) 1034–1074.
[18] R.N. da Silva, A.C. Tomé, J.P.C. Tomé, M.G.P.M.S. Neves, M.A.F. Faustino, J.A. S. Cavaleiro, A. Oliveira, A. Almeida, Â. Cunha, Photo-inactivation of Bacillus endospores: inter-specific variability of inactivation efficiency, Microbiol. Immunol. 56 (2012) 692–699.
[19] T. Maisch, C. Bosl, R.M. Szeimies, B. Love, C. Abels, Determination of the antibacterial efficacy of a new porphyrin-based photosensitizer against MRSA ex vivo, Photochem. Photobiol. Sci. 6 (2007) 545.
[20] G.B. Rodrigues, L.K.S. Ferreira, M. Wainwright, G.U.L. Braga, Susceptibilities of the dermatophytes Trichophyton mentagrophytes and T. rubrum microconidia to photodynamic antimicrobial chemotherapy with novel phenothiazinium photosensitizers and red light, J. Photochem. Photobiol., B 116 (2012) 89–94.
[21] G.B. Rodrigues, M. Dias-Baruffi, N. Holman, M. Wainwright, G.U.L. Braga, In vitro photodynamic inactivation of Candida species and mouse fibroblasts with phenothiaziniumphotosensitisers and red light, Photodiagn. Photodyn. Ther. 10 (2013) 141–149.
[22] Sandra Beirao, S. Fernandes, J. Coelho, M.A.F. Faustino, J.P.C. Tome, M. Neves, A. C. Tome, A. Almeida, A. Cunha, Photodynamic inactivation of bacterial and yeast biofilms with a cationic porphyrin, Photochem. Photobiol. 90 (6) (2014) 1387–1396.
[23] R. Fekrazad, Photobiomodulation and Antiviral Photodynamic Therapy as a Possible Novel Approach in COVID-19 Management, Photobiomodul., Photomed., Laser Surg. 38 (2020) 255–257.
[24] R.R. Allison, C.H. Sibata, Oncologic photodynamic therapy photosensitizers: A clinical review, Photodiagn. Photodyn. Ther. 7 (2010) 61–75.
[25] H. Abrahamse, R. Michael, Hamblin, New photosensitizers for photodynamic therapy, Biochem. J. 473 (2016) 347–364.
[26] H. Chung, T. Dai, S.K. Sharma, Y.-Y. Huang, J.D. Carroll, M.R. Hamblin, The Nuts and Bolts of Low-level Laser (Light) Therapy, Ann. Biomed. Eng. 40 (2011) 516–533.
[27] Liyi Huang, et al., Paradoxical potentiation of methylene blue-mediated antimicrobial photodynamic inactivation by sodium azide: role of ambient oxygen and azide radicals, Free Radical Biol. Med. 53 (11) (2012) 2062–2071.
[28] Maurício S. Baptista, et al., Type I and type II photosensitized oxidation reactions: guidelines and mechanistic pathways, Photochem. Photobiol. 93 (4) (2017) 912–919.
[29] R. Tao, F. Zhang, Q.-J. Tang, C.-S. Xu, Z.-J. Ni, X.-H. Meng, Effects of curcumin-based photodynamic treatment on the storage quality of fresh-cut apples, Food Chem. 274 (2019) 415–421.
[30] C.C.C. Quishida, E.G. De Oliveira Mima, J.H. Jorge, C.E. Vergani, V.S. Bagnato, A. C. Pavarina, Photodynamic inactivation of a multispecies biofilm using curcumin and LED light, Lasers Med. Sci. 31 (2016) 997–1009.
[31] M. Mirzahosseinipour, K. Khorsandi, R. Hosseinzadeh, M. Ghazaeian, F.K. Shahidi, Antimicrobial photodynamic and wound healing activity of curcumin encapsulated in silica nanoparticles, Photodiagn. Photodyn. Ther. 29 (2020), 101639.
[32] D. Praditya, L. Kirchhoff, J. Brüning, H. Rachmawati, J. Steinmann, E. Steinmann, Anti-infective Properties of the Golden Spice Curcumin, Front. Microbiol. 10 (2019).
[33] W.H. Tsai, K.-H. Yu, Y.-C. Huang, C.-I. Lee, EGFR-targeted photodynamic therapy by curcumin-encapsulated chitosan/TPP nanoparticles, Int. J. Nanomed. 13 (2018) 903–916.
[34] R.K. Maheshwari, A.K. Singh, J. Gaddipati, R.C. Srimal, Multiple biological activities of curcumin: A short review, Life Sci. 78 (2006) 2081–2087.
[35] G. Bar-Sela, R. Epelbaum, M. Schaffer, Curcumin as an Anti-Cancer Agent: Review of the Gap Between Basic and Clinical Applications, Curr. Med. Chem. 17 (2010) 190–197.
[36] P. Basnet, N. Skalko-Basnet, Curcumin: An Anti-Inflammatory Molecule from a Curry Spice on the Path to Cancer Treatment, Molecules 16 (2011) 4567–4598.
[37] T. Hamaguchi, K. Ono, M. Yamada, REVIEW: Curcumin and Alzheimer's Disease, CNS Neurosci. Ther. 16 (2010) 285–297.
[38] A. Federico, E. Cardaioli, P. Da Pozzo, P. Formichi, G.N. Gallus, E. Radi, Mitochondria, oxidative stress and neurodegeneration, J. Neurol. Sci. 322 (2012) 254–262.
[39] V. Sakima, P. Barbugli, P. Cerri, M. Chorilli, J. Carmello, A. Pavarina, E. Mima, Antimicrobial Photodynamic Therapy Mediated by Curcumin-Loaded Polymeric Nanoparticles in a Murine Model of Oral Candidiasis, Molecules 23 (2018) 2075.
[40] D. Akbik, M. Ghadiri, W. Chrzanowski, R. Rohanizadeh, Curcumin as a wound healing agent, Life Sci. 116 (2014) 1–7.
[41] B. Fonseca-Santos, A.M. dos Santos, C.F. Rodero, M.P.D. Gremião, M. Chorilli, Design, characterization, and biological evaluation of curcumin-loaded surfactant-based systems for topical drug delivery, Int. J. Nanomed. 11 (2016) 4553–4562.
[42] S. Tejada, A. Manayi, M. Daglia, S.F. Nabavi, A. Sureda, Z. Hajheydari, O. Gortzi, H. Pazoki-Toroudi, S.M. Nabavi, Wound Healing Effects of Curcumin: A Short Review, Curr. Pharm. Biotechnol. 17 (2016) 1002–1007.
[43] Z. Hussain, H.E. Thu, S.-F. Ng, S. Khan, H. Katas, Nanoencapsulation, an efficient and promising approach to maximize wound healing efficacy of curcumin: A review of new trends and state-of-the-art, Colloids Surf., B 150 (2017) 223–241.
[44] Y. Jiang, A.W. Leung, H. Hua, X. Rao, C. Xu, Photodynamic Action of LED-Activated Curcumin against Staphylococcus aureus Involving Intracellular ROS Increase and Membrane Damage, Int. J. Photoenergy 2014 (2014) 1–7.

[45] T. Dai, G.P. Tegos, T. Zhiyentayev, E. Mylonakis, M.R. Hamblin, Photodynamic therapy for methicillin-resistant Staphylococcus aureus infection in a mouse skin abrasion model, Lasers Surg. Med. 42 (2010) 38–44.
[46] S. Khan, F. Alam, A. Azam, A.U. Khan, Gold nanoparticles enhance methylene blue induced photodynamic therapy: a novel therapeutic approach to inhibit Candida albicans biofilm, Int. J. Nanomed. 3245 (2012).
[47] J.P.M.L. Rolim, M.A.S. de-Melo, S.F. Guedes, F.B. Albuquerque-Filho, J.R. de Souza, N.A.P. Nogueira, I.C.J. Zanin, L.K.A. Rodrigues, The antimicrobial activity of photodynamic therapy against Streptococcus mutans using different photosensitizers, J. Photochem. Photobiol. B: Biol., 106 (2012) 40-46.
[48] L. Misba, S. Kulshrestha, A.U. Khan, Antibiofilm action of a toluidine blue O-silver nanoparticle conjugate on Streptococcus mutans: a mechanism of type I photodynamic therapy, Biofouling 32 (2016) 313–328.
[49] K.R. Kasimova, M. Sadasivam, G. Landi, T. Sarna, M.R. Hamblin, Potentiation of photoinactivation of Gram-positive and Gram-negative bacteria mediated by six phenothiazinium dyes by addition of azide ion, Photochem. Photobiol. Sci. 13 (2014) 1541–1548.
[50] J. Chen, T.C. Cesario, P.M. Rentzepis, Rationale and mechanism for the low photoinactivation rate of bacteria in plasma, Proc. Natl. Acad. Sci. 111 (2013) 33–38.
[51] L. Misba, S. Zaidi, A.U. Khan, A comparison of antibacterial and antibiofilm efficacy of phenothiazinium dyes between Gram positive and Gram negative bacterial biofilm, Photodiagn. Photodyn. Ther. 18 (2017) 24–33.
[52] A. López-Moreno, J.D. Sepúlveda-Sánchez, E.M. Mercedes Alonso Guzmán, S. Le Borgne, Calcium carbonate precipitation by heterotrophic bacteria isolated from biofilms formed on deteriorated ignimbrite stones: influence of calcium on EPS production and biofilm formation by these isolates, Biofouling, 30 (2014) 547-560.
[53] S. Kulshrestha, S. Khan, S. Hasan, M.E. Khan, L. Misba, A.U. Khan, Calcium fluoride nanoparticles induced suppression of Streptococcus mutans biofilm: an in vitro and in vivo approach, Appl. Microbiol. Biotechnol. 100 (2015) 1901–1914.
[54] V.A. Senapati, A. Kumar, G.S. Gupta, A.K. Pandey, A. Dhawan, ZnO nanoparticles induced inflammatory response and genotoxicity in human blood cells: A mechanistic approach, Food Chem. Toxicol. 85 (2015) 61–70.
[55] F. Gad, T. Zahra, K.P. Francis, T. Hasan, M.R. Hamblin, Targeted photodynamic therapy of established soft-tissue infections in mice, Photochem. Photobiol. Sci. 3 (2004) 451.
[56] J.H. Park, M.-Y. Ahn, Y.-C. Kim, S.-A. Kim, Y.-H. Moon, S.-G. Ahn, J.-H. Yoon, In Vitro and in Vivo Antimicrobial Effect of Photodynamic Therapy Using a Highly Pure Chlorin e6 against Staphylococcus aureus Xen29, Biol. Pharm. Bull. 35 (2012) 509–514.
[57] A.A. Tawfik, I. Noaman, H. El-Elsayyad, N. El-Mashad, M. Soliman, A study of the treatment of cutaneous fungal infection in animal model using photoactivated composite of methylene blue and gold nanoparticle, Photodiagn. Photodyn. Ther. 15 (2016) 59–69.
[58] M. Karamese, H.S. Erol, M. Albayrak, G. FindikGuvendi, E. Aydin, S. AksakKaramese, Anti-oxidant and anti-inflammatory effects of apigenin in a rat model of sepsis: an immunological, biochemical, and histopathological study, Immunopharmacol. Immunotoxicol. 38 (2016) 228–237.
[59] ANOVA: ANalysis Of VAriance between groups. www.physics.csbsju.edu/stats/anova.html.
[60] G.L. Archer, Staphylococcus aureus: A Well-Armed Pathogen, Clin. Infect. Dis. 26 (1998) 1179–1181.
[61] A.S. Bayer, A.F. Bolger, K.A. Taubert, W. Wilson, J. Steckelberg, A.W. Karchmer, M. Levison, H.F. Chambers, A.S. Dajani, M.H. Gewitz, J.W. Newburger, M. A. Gerber, S.T. Shulman, T.J. Pallasch, T.W. Gage, P. Ferrieri, Diagnosis and Management of Infective Endocarditis and Its Complications, Circulation 98 (1998) 2936–2948.
[62] B.M. Limbago, A.J. Kallen, W. Zhu, P. Eggers, L.K. McDougal, V.S. Albrecht, Report of the 13th Vancomycin-Resistant Staphylococcus aureus Isolate from the United States, J. Clin. Microbiol. 52 (2013) 998–1002.
[63] A. FriÃEs, C. Resina, V. Manuel, L. Lito, M. Ramirez, J. Melo-Cristino, Epidemiological survey of the first case of vancomycin-resistant Staphylococcus aureus infection in Europe, Epidemiol. Infect. 143 (2014) 745–748.
[64] P.P. Almeida, Í.S. Pereira, K.B. Rodrigues, L.S. Leal, A.S. Marques, L.P. Rosa, F.C. da Silva, R.A.A. da Silva, Photodynamic therapy controls of Staphylococcus aureus intradermal infection in mice, Lasers Med. Sci. 32 (2017) 1337–1342.
[65] D.J. Diekema, B.J. BootsMiller, T.E. Vaughn, R.F. Woolson, J.W. Yankey, E.J. Ernst, S.D. Flach, M.M. Ward, C.L.J. Franciscus, M.A. Pfaller, B.N. Doebbeling, Antimicrobial Resistance Trends and Outbreak Frequency in United States Hospitals, Clin. Infect. Dis. 38 (2004) 78–85.
[66] S. Projan, Antimicrobials: new solutions badly needed, Curr. Opin. Microbiol. 5 (2002) 463–465.
[67] K. Sieradzki, R.B. Roberts, S.W. Haber, A. Tomasz, The Development of Vancomycin Resistance in a Patient with Methicillin-ResistantStaphylococcusaureusInfection, N. Engl. J. Med. 340 (1999) 517–523.
[68] S. Khan, S.N. Khan, R. Meena, A.M. Dar, R. Pal, A.U. Khan, Photoinactivation of multidrug resistant bacteria by monomeric methylene blue conjugated gold nanoparticles, J. Photochem. Photobiol., B 174 (2017) 150–161.
[69] Z.A. Malik, D. Broughel, The importance of testing whole stool for Shiga toxin: a clinical and microbiological perspective, J.-Pakistan Med. Assoc. 57 (5) (2007) 265.
[70] G.P. Tegos, M. Anbe, C. Yang, T.N. Demidova, M. Satti, P. Mroz, S. Janjua, F. Gad, M.R. Hamblin, Protease-Stable Polycationic Photosensitizer Conjugates between Polyethyleneimine and Chlorin(e6) for Broad-Spectrum Antimicrobial Photoinactivation, Antimicrob. Agents Chemother. 50 (2006) 1402–1410.
[71] M.R. Hamblin, Polycationic photosensitizer conjugates: effects of chain length and Gram classification on the photodynamic inactivation of bacteria, J. Antimicrob. Chemother. 49 (2002) 941–951.
[72] G.A. Pankey, L.D. Sabath, Clinical Relevance of Bacteriostatic versus Bactericidal Mechanisms of Action in the Treatment of Gram-Positive Bacterial Infections, Clin. Infect. Dis. 38 (2004) 864–870.
[73] S.Y. Kim, O.J. Kwon, J.-W. Park, Inactivation of catalase and superoxide dismutase by singlet oxygen derived from photoactivated dye, Biochimie 83 (2001) 437–444.
[74] C. Liu, Y. Zhou, L. Wang, L. Han, J.e. Lei, H.M. Ishaq, S.P. Nair, J. Xu, Photodynamic inactivation of Klebsiellapneumoniae biofilms and planktonic cells by 5-aminolevulinic acid and 5-aminolevulinic acid methyl ester, Lasers Med. Sci., 31 (2016) 557-565.
[75] A. Zuberi, N. Ahmad, A.U. Khan, CRISPRi Induced Suppression of Fimbriae Gene (fimH) of a Uropathogenic Escherichia coli: An Approach to Inhibit Microbial Biofilms, Front. Immunol. 8 (2017).
[76] H.C. Flemming, J. Wingender, The biofilm matrix, Nat. Rev. Microbiol. 8 (2010) 623–633.
[77] J.J. Burns, L. Zhao, E.W. Taylor, K. Spelman, The influence of traditional herbal formulas on cytokine activity, Toxicology 278 (2010) 140–159.
[78] J. Šventoraitytė, A. Žvirblienė, G. Kiudelis, R. Žalinkevičius, A. Žvirblienė, A. Praškevičius, L. Kupčinskas, V. Tamošiūnas, Immune system alterations in patients with inflammatory bowel disease during remission, Medicina 44 (2008) 27.
[79] J.V. Fahy, Type 2 inflammation in asthma present in most, absent in many, Nat. Rev. Immunol. 15, (1) (2015) 57-65.